Decoupling of iron and phosphate in the global ocean

P. Parekh, M. J. Follows, and E. A. Boyle

Department of Earth, Atmospheric and Planetary Sciences, Massachusetts Institute of Technology, Cambridge, Massachusetts, USA

Received 12 April 2004; revised 17 January 2005; accepted 16 March 2005; published 7 May 2005.

[1] We formulate a mechanistic model of the coupled oceanic iron and phosphorus cycles. The iron parameterization includes scavenging onto sinking particles, complexation with an organic ligand, and a prescribed aeolian source. Export production is limited by the availability of light, phosphate, and iron. We implement this biogeochemical scheme in a coarse resolution ocean general circulation model using scavenging rates and conditional stability constants guided by laboratory studies and a suite of box model sensitivity studies. The model is able to reproduce the broad regional patterns of iron and phosphorus. In particular, the high macronutrient concentrations of the Southern Ocean, tropical Pacific, and subarctic Pacific emerge from the explicit iron limitation of the model. In addition, the model also qualitatively reproduces the observed interbasin gradients of deep, dissolved iron with the lowest values in the Southern Ocean. The ubiquitous presence of significant amounts of free ligand is also explicitly captured. We define a tracer, Fe^* which quantifies the degree to which a water mass is iron limited, relative to phosphorus. Surface waters in high-nutrient, low-chlorophyll regions have negative Fe^* values, indicating Fe limitation. The extent of the decoupling of iron and phosphorus is determined by the availability and binding strength of the ligand relative to the scavenging by particulate. Global iron concentrations are sensitive to changes in scavenging rate and physical forcing. Decreasing the scavenging rate 40% results in $\sim$0.1 nM increase in dissolved iron in deep waters. Forcing the model with weaker wind stresses leads to a decrease in surface $[PO_4]$ and $[Fe]$ in the Southern Ocean due to a reduction in the upwelling strength.

Citation: Parekh, P., M. J. Follows, and E. A. Boyle (2005), Decoupling of iron and phosphate in the global ocean, *Global Biogeochem. Cycles*, *19*, GB2020, doi:10.1029/2004GB002280.

1. Introduction

[2] In recent years, iron has been recognized and examined as a key element in ocean biogeochemical cycles. *Martin and Fitzwater* [1988] highlighted the role of iron as the limiting nutrient for phytoplankton growth in the "high-nutrient, low-chlorophyll" (HNLC) regions of the oceans. The HNLC regions, with elevated, unutilized surface macronutrients, include the high-latitude Southern Ocean, the equatorial Pacific, and the North Pacific. The abundance and availability of iron in the ocean is controlled by a complex set of processes including biological utilization and export, interactions with particulate matter and complexing organic molecules, and aeolian deposition of iron-rich dust. Since iron is quickly stripped from the water column, it is present in very low concentrations and depleted relative to macronutrients in some upwelling regions [*Measures and Vink*, 2001]. The aeolian source of iron may partially compensate but is small in some remote ocean regions [e.g., *Gao et al.*, 2001]. *Martin* [1990] speculated that enhanced dust transport to the remote Southern Ocean during glacial periods, as inferred from ice cores [*Petit et al.*, 1999] might fertilize the region, enhance the global biological carbon pump, and draw down atmospheric CO_2. Additionally, nitrogen fixing organisms (reviewed by *Karl et al.* [2002] and *Mills et al.* [2004]) have a greater iron requirement, and iron availability and dust transport may also regulate the ocean's nitrogen budget [*Michaels et al.*, 1996; *Falkowski*, 1997].

[3] The recognition of the key role of iron has further stimulated the efforts to observe and map the distribution of iron in the world's oceans [*de Jong et al.*, 1998; *Wu and Boyle*, 1998; *Johnson et al.*, 2000; *Weeks and Bruland*, 2002]. We illustrate the distribution inferred from the still sparse ocean observations in Figure 1 (expanded from *Gregg et al.*, 2003; *de Baar and de Jong*, 2001; *Johnson et al.*, 1997]. The total "dissolved" iron concentration is typically defined as that which passes through a 0.40- or 0.20-micron filter. In practice, this includes iron in several forms. Laboratory and field studies have indicated that the majority of total dissolved iron, Fe_T, is complexed with

0886-6236/05/2004GB002280$12.00

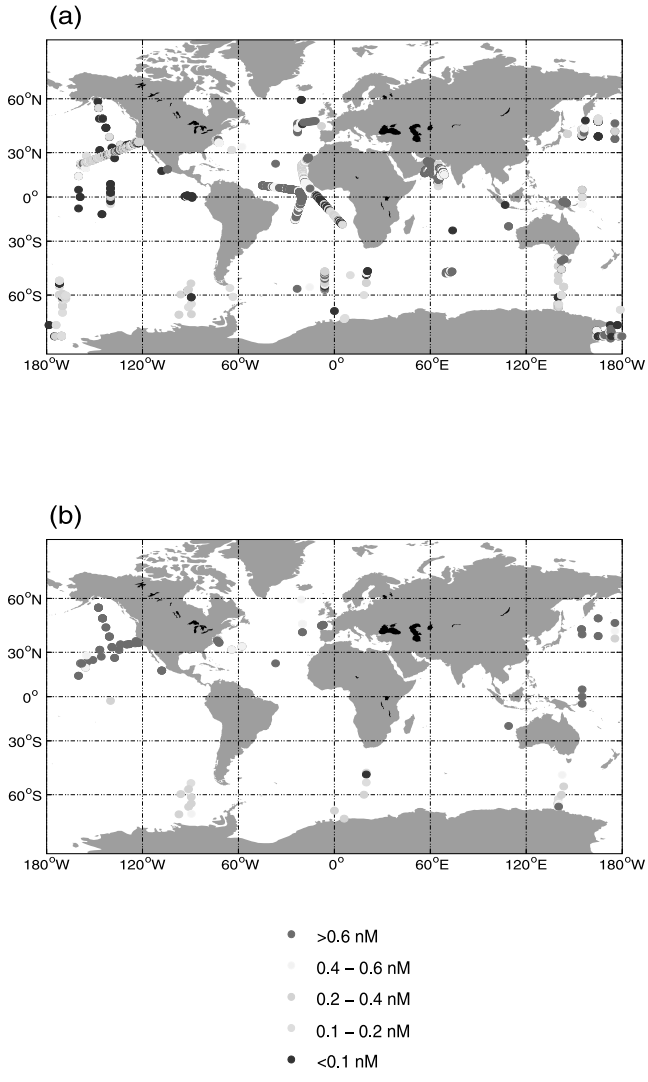

Figure 1. (a) Observed dissolved [*Fe*] (<0.4 μm) in surface waters (0 to 50 m) and (b) intermediate waters (800–1100 m). We have expanded the *Gregg et al.* [2003], *de Baar and de Jong* [2001], and *Johnson et al.* [1997] databases. References are found in Appendix A. The annotated and fully referenced data set is available for downloading at ocean.mit.edu/∼mick/Downloads.html. See color version of this figure at back of this issue.

organic ligands, *L*, which might protect it from scavenging and precipitation [*Gledhill and van den Berg*, 1994; *Rue and Bruland*, 1995; *van den Berg*, 1995; *Wu and Luther*, 1995; *Rue and Bruland*, 1997; *Gledhill et al.*, 1998; *Nolting et al.*, 1998; *Witter and Luther*, 1998; *Witter et al.*, 2000a; *Boye et al.*, 2001].

[4] Estimates of the concentration of ligand range between 0.5 and 6 nM. The estimated conditional stability constant of the ligand(s) (K_{FeL}) ranges between $10^{9.8}$ M^{-1} and $10^{14.3}$ M^{-1} without any clear regional pattern. Most studies suggest only one class of active organic ligand, but two studies [*Rue and Bruland*, 1997; *Nolting et al.*, 1998] have inferred two ligand classes, in the North Pacific and the Pacific sector of the Southern Ocean, hypothesizing that the stronger ligand class is produced biologically while the weaker ligand is a degradation product. Typically, there is observed to be an excess of free, uncomplexed ligand, L', in oceanic waters. Recent studies have also shown that a significant fraction of Fe_T is in colloidal form [*Wells et al.*, 1995; *Wu et al.*, 2001; *Nishioka et al.*, 2001, 2003]. The bioavailability of colloidal particles is not yet known, and they might aggregate into larger particles that sink out of the water column [*Honeyman and Santschi*, 1989].

[5] In situ iron fertilization studies have been carried out in open ocean HNLC regions [*Martin et al.*, 1994; *Coale et al.*, 1996a; *Boyd et al.*, 2000; *Tsuda et al.*, 2003; *Boyd et al.*, 2004; *Coale et al.*, 2004] and have clearly demonstrated a response in primary production to the addition of iron. Early studies were not able to conclusively indicate any associated increase in export of carbon [*Charette and Buesseler*, 2000]. This may be, in part, due to the logistical difficulties of monitoring the fertilized patch over sufficiently long periods of time. More recently, there is evidence of increased export production as a response to iron fertilization [*Boyd et al.*, 2004; *Buesseler et al.*, 2004]. *Buesseler et al.* [2004] found particulate organic carbon (POC) fluxes of ∼20% of biological carbon uptake at 100 m at the end of the 28-day observation period in the Southern Ocean, while *Boyd et al.* [2004] found 8% of POC lost from the mixed layer present at ∼120 m in the Gulf of Alaska after 24 days.

1.1. Models of the Oceanic Iron Cycle

[6] Numerical models provide a means to synthesize, encapsulate, and test the community's qualitative and quantitative understanding of biogeochemical cycles. The ability of a model, based on the proposed parameterizations and rate coefficients, can reproduce key features of the observed data, as well as lend support to the underlying assumptions and understanding. Such models may also be used to explore the sensitivities of the system to changes in forcing, parameterizations, or parameter values.

[7] There are, as yet, only a few published model studies focusing specifically on the global scale ocean iron cycle over the whole water column. *Leféevre and Watson* [1999] and *Archer and Johnson* [2000], using box model and three-dimensional general circulation model (GCM) frameworks, respectively, developed conceptually similar models. In both cases the source of iron to the ocean is aeolian deposition and the sink is represented as rapid scavenging of any dissolved iron not complexed to organic ligands. In both cases it was assumed that the organic ligand is present in the ocean with concentration of 0.6 nM and that it is, by and large, saturated. *Leféevre and Watson* [1999] represented this in a highly idealized form, relaxing the dissolved iron concentration toward 0.6 nM. *Archer and Johnson* [2000] explicitly represented a ligand, with concentration of 0.6 nM, and imposed a relatively strong conditional stability coefficient such that the ligand is effectively saturated. In both models, the deep ocean distribution of iron was uniformly close to 0.6 nM, essentially representing the complexed pool, and consistent with then current interpre-

tations of the oceanic observations. (*Archer and Johnson* [2000] also explored a system with two organic ligands: one strongly and one weakly complexing.)

[8] More recently, however, the growing number of oceanic observations suggests that the deep ocean iron distribution does show interbasin gradients with highest concentrations in the North Atlantic, lower in the Southern Ocean and central Pacific and Northern Pacific values approaching those in the Atlantic (Figure 1b). In regions of relatively strong aeolian supply, such as the North Atlantic and Indian oceans, surface [Fe_T] is elevated (Figure 1a). *Landing et al.* [2004] have observed [Fe_T] as high as 1.5 nM in the surface waters of the Atlantic. Surface [Fe_T] appear lower, but not negligible, in the Southern Ocean. In addition, more recent measurements of ligand concentration suggest that ligand concentrations (although quite variable) are typically between 0.5 and 6 nM [*Gledhill and van den Berg*, 1994; *Rue and Bruland*, 1995; *van den Berg*, 1995; *Wu and Luther*, 1995; *Rue and Bruland*, 1997; *Gledhill et al.*, 1998; *Nolting et al.*, 1998; *Witter and Luther*, 1998; *Witter et al.*, 2000a; *Boye et al.*, 2001; *Powell and Donat*, 2001] and, unlike in the prior models, the ligand is not typically saturated.

[9] In the framework of an idealized, global ocean box model [*Parekh et al.*, 2004], we have recently examined the ability of three different parameterizations of ocean iron cycling to reproduce the interbasin gradients in the deep waters as revealed in Figure 1b. A model in which iron is scavenged onto particles and complexed with an organic ligand, in accord with the conceptual view of *Johnson et al.* [1997] and similar to that of *Archer and Johnson* [2000] was consistent with the limited observational constraints provided an appropriate ratio of scavenging rate, k_{sc} and conditional stability constant, K_{FeL} (the binding strength of the ligand), was imposed. By applying a weaker, yet still plausible, conditional stability constant, and a higher total ligand concentration than in the previously published studies [*Lefèvre and Watson*, 1999; *Archer and Johnson*, 2000], we were able to reproduce the recently observed features of the iron cycle. These include the basin to basin contrasts in Fe_T, with low concentrations in the deep Southern Ocean, and the ubiquitous presence of iron-free organic ligand which were more recently observed and not captured in the earlier models.

[10] In addition, several model studies have represented iron cycling in order to consider the impact of upper ocean iron availability and iron limitation of the ecosystem [*Moore et al.*, 2002; *Christian et al.*, 2002; *Aumont et al.*, 2003; *Gregg et al.*, 2003]. The main focus of these studies is how the iron distribution impacts the ecosystem and not what sets that distribution. Such models have typically employed a parameterization of iron scavenging similar to that of *Lefèvre and Watson* [1999] or *Johnson et al.* [1997] in which dissolved iron in excess of an assumed ligand concentration of 0.6 nM is rapidly lost.

1.2. Aims of This Study

[11] The results of our box model study [*Parekh et al.*, 2004] suggest that the current picture of the oceanic iron distribution, with low Southern Ocean deep iron concentrations, along with observations of higher ligand concentrations and ubiquitous free ligand, can be captured using an iron model with parameterizations of scavenging and complexation. It suggests that a framework similar to that applied by *Archer and Johnson* [2000], though not in the saturated ligand limit, may provide a better description of the more recent data. In addition, the box model suggested that the sensitivity to changes in aeolian iron supply is very different in the models representing complexation, in contrast to those which are purely scavenging based. Here, then, we present a three-dimensional circulation and biogeochemistry model focusing on the coupled oceanic iron and phosphorus cycles. The iron cycle is parameterized with representations of both scavenging and complexation with the ratio of scavenging rate to conditional stability coefficient, k_{sc}/K_{FeL}, determined from the optimal box model case, with total ligand concentrations of 1 nM or greater. We will demonstrate that this model can reproduce the broad features of the oceanic iron distribution, captures the presence of free ligand, and explicitly leads to "HNLC" regions, with elevated surface nutrients, in the model. In the following sections we will outline the structure and mechanics of the ocean general circulation biogeochemistry model, discuss model results and compare to observations, define a new tracer to assess Fe limitation, and present the sensitivity of Fe_T to scavenging rate and wind stresses.

2. Global Ocean Biogeochemistry Model

2.1. Physical Model

[12] We overlay coupled iron and phosphorus cycle models on the MIT ocean circulation model [*Marshall et al.*, 1997a, 1997b; *Adcroft et al.*, 1997] configured globally at coarse resolution (2.8 × 2.8 degrees, 15 vertical levels). The uppermost layers of the model are 50 m, 70 m, and 100 m thick. The physical model is forced with a climatological annual cycle of surface wind stresses [*Trenberth et al.*, 1989], surface heat, and freshwater fluxes with additional relaxation toward climatological sea surface temperature and salinity. In these coarse resolution studies, the effect of mesoscale eddy transfers is parameterized following *Gent and McWilliams* [1990]. Vertical turbulent mixing in the surface mixed layer of the ocean is represented through a simple convective adjustment scheme. This configuration of the ocean model is similar to that employed in the Ocean Carbon Model Intercomparison Project (OCMIP) to simulate the ventilation of chlorofluorocarbons [*Dutay et al.*, 2002] and aspects of the ocean carbon cycle [e.g., *Watson and Orr*, 2003; *Matsumoto et al.*, 2004]. The configuration of the MIT model applied here differs from that of the OCMIP study only in the surface wind stress forcing: The *Trenberth et al.* [1989] wind stress applied here leads to a more vigorous Drake Passage throughflow and Southern Ocean residual overturning circulation than in the OCMIP configuration (presented by *Doney et al.* [2004]) which used *Hellerman and Rosenstein* [1983] climatological wind stress forcing.

[13] Figure 2 shows the model's annual mean, "residual" overturning circulation: the net effect of advection by mean flow and a contribution due to eddies. The strong Northern

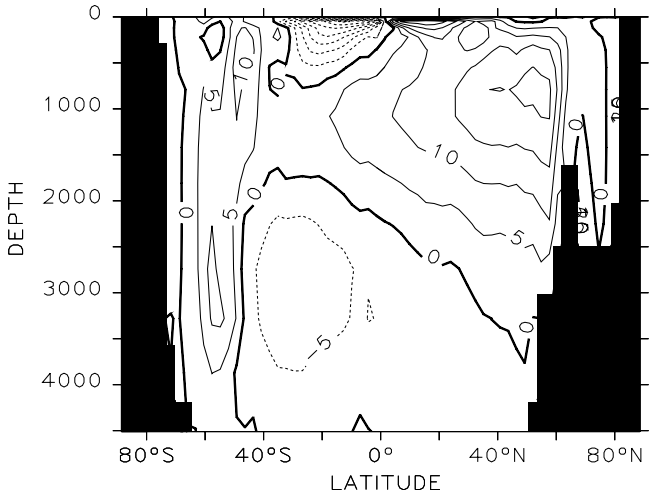

Figure 2. Residual mean overturning circulation of the model (*Trenberth et al.* [1989] wind stress forcing). Fluxes are in Sv (10^6 m^3 s^{-1}).

Hemisphere overturning cell reflects the strong influence of the Atlantic basin, with the formation of North Atlantic Deep Water in the north, its transit southward at mid-depths, and return flow in the surface waters. There is a residual overturning in the Southern Ocean of the model, associated with upwelling of deep waters and formation of intermediate waters, though it is weaker than estimates of the meridional overturning circulation interpreted from hydrographic data with idealized theories *Karsten and Marshall*, 2002] and inferred from transient tracers [*Ito et al.*, 2004]. However, it is significantly stronger in this case than in the original OCMIP configuration [*Doney et al.*, 2004]. The deep cell in the opposing sense reflects the formation of bottom waters in the southern polar region, their upwelling in the interior, and return southward at mid-depths. This cell dominates the deep Atlantic circulation and much of the Pacific basin.

2.2. Biogeochemical Model

[14] We model the coupled phosphorus and iron cycles, using a simplified parameterization of export production in which biological uptake and regeneration are indexed to phosphorus. Figure 3 indicates the biogeochemical processes acting on both phosphorus and iron in the model. While both are consumed, exported, and regenerated in association with biological activity, iron is decoupled from phosphorus in the ocean due to the additional processes of scavenging and complexation, and its significant aeolian source. Model parameter values are given in Table 1.

2.2.1. Phosphorus Cycle

[15] The governing equations for phosphate, PO_4, and dissolved organic phosphorus, DOP, in the euphotic zone (h_e = 120 m) of the biogeochemical model are

$$\frac{\partial PO_4}{\partial t} = -\bigtriangledown\cdot(\mathbf{u}PO_4) + \bigtriangledown\cdot(\kappa\bigtriangledown PO_4) - \Gamma + \lambda\mathrm{DOP}, \quad (1)$$

$$\frac{\partial \mathrm{DOP}}{\partial t} = -\bigtriangledown\cdot(\mathbf{u}\mathrm{DOP}) + \bigtriangledown\cdot(\kappa\bigtriangledown \mathrm{DOP}) + \nu\Gamma - \lambda\mathrm{DOP}, \quad (2)$$

$$\Gamma = \alpha\frac{PO_4}{PO_4 + K_{PO4}}\frac{Fe_T}{Fe_T + K_{Fe}}\frac{I}{I + K_I}, \quad (3)$$

where **u** is the transformed Eulerian mean velocity and κ is a mixing tensor representing isopycnal mixing following *Gent and McWilliams* [1990]. We use a second-order flux limiter advection scheme for tracers [*Roe*, 1985]. Γ represents the biological uptake, which is limited by light, phosphate, and iron. The maximum export rate (α) is set to 0.5 μM month^{-1}. Iron and phosphate limitation are represented by Michaelis-Menten kinetics. The half saturation constant for iron (K_{Fe}) is 0.12 nM, within the range of measured values [*Price et al.*, 1994; *Fitzwater et al.*, 1996], while the half saturation constant for phosphate (K_{PO4}) is 0.5 μM, which leads to reasonable modeled surface [PO_4] and [Fe_T] distributions. A fraction, ν = 0.67, of nutrients lost from the surface layer enters the surface DOP pool, which has an e-folding timescale for remineralization, 1/λ, of 6 months [following *Yamanaka and Tajika*, 1997]. Below the euphotic zone, the governing equations are

$$\frac{\partial PO_4}{\partial t} = -\bigtriangledown\cdot(\mathbf{u}PO_4) + \bigtriangledown\cdot(\kappa\bigtriangledown PO_4) + \lambda DOP - \frac{\partial F(z)}{\partial z}, \quad (4)$$

$$\frac{\partial DOP}{\partial t} = -\bigtriangledown\cdot(\mathbf{u}DOP) + \bigtriangledown\cdot(\kappa\bigtriangledown DOP) - \lambda DOP, \quad (5)$$

$$Export = \int_{h_e}^{0}(1-\nu)\Gamma dz, \quad (6)$$

$$F(z) = Export\left(\frac{z}{h_e}\right)^{-b}. \quad (7)$$

[16] Here the remaining fraction of consumed phosphorus, [$(1-\nu)\,\Gamma$], is instantaneously exported as particulate to depth [*Yamanaka and Tajika*, 1997] where it is remineralized according to the empirical power law relationship determined by *Martin et al.* [1987]. Any remaining particulate organic matter that reaches the bottom of the model domain is instantly remineralized. Insolation varies as a function of latitude and season following the astronomical formula of *Paltridge and Platt* [1976]. We set the half saturation value for light (I_0) to 30 W m^{-2}.

2.3. Iron Parameterizations

[17] The governing equation for total dissolved iron (Fe_T) in the model is

$$\frac{dFe_T}{dt} = S_{Fe} - \bigtriangledown\cdot(\mathbf{u}Fe_T) + \bigtriangledown\cdot(\kappa\bigtriangledown Fe_T) - \Gamma R_{Fe} + \lambda DOPR_{Fe} + J_{Fe}. \quad (8)$$

[18] S_{Fe} represents external sources of iron to the ocean. These include aeolian deposition [*Duce and Tindale*, 1991], riverine inputs, hydrothermal activity, and continental margin sediments [*Hutchins and Bruland*, 1998; *Johnson et al.*, 1999; *Elrod et al.*, 2004]. Here we impose only an aeolian

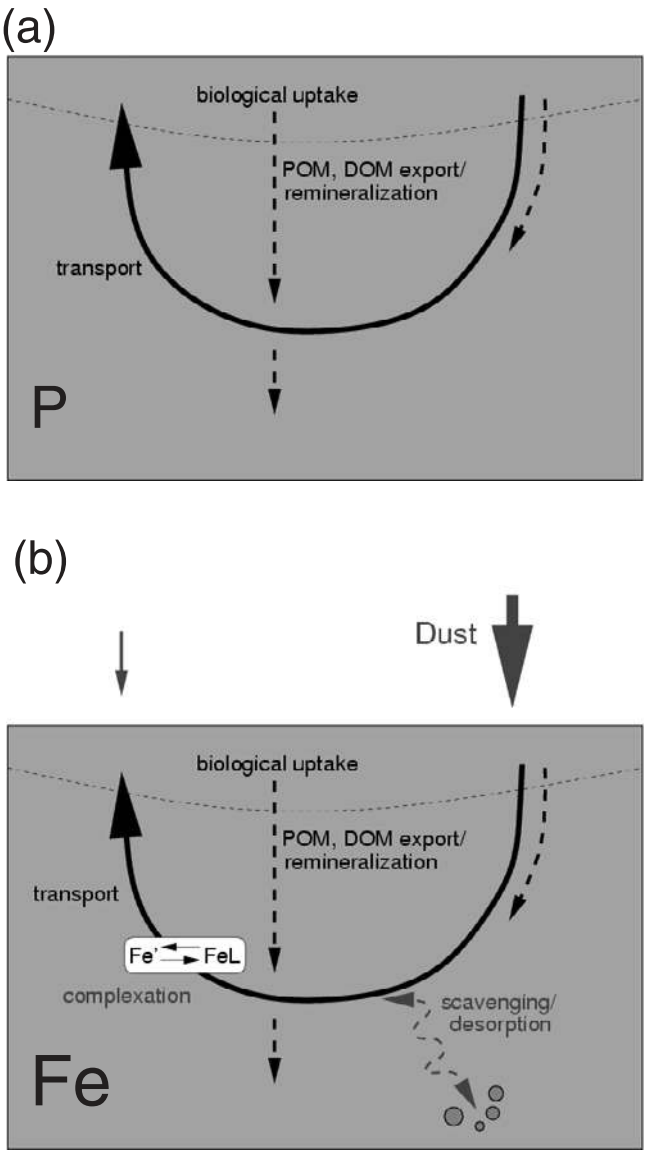

Figure 3. Schematic representation of the modeled phosphorus and iron cycles. Both phosphorus and iron are utilized biologically in the surface ocean and exported in either particulate or dissolved organic matter to the interior ocean, where they are remineralized. Their cycles are decoupled through the additional processes acting on iron, including scavenging onto sinking particles, complexation with organic ligands, and the significant aeolian source.

source based on modeled estimates of monthly dust flux generated from an atmospheric transport model [*Luo et al.*, 2003] (Figure 4). We assume that iron is 3.5 weight% of the dust. $S_{Fe} = \beta F_{in}$, where β is the solubility of Fe aerosols in seawater which is not well known. *Jickells and Spokes* [2001] suggest it ranges between 0.8 and 2.1%, assuming 30% contribution from wet deposition (with solubility ranging between 0.3 and 6.8%) and 70% dry deposition with negligible solubility. On the basis of sensitivity studies with a box model [*Parekh et al.*, 2004], we set $\beta = 0.01$ in all the model runs discussed here. This is a significant unknown parameter and is unlikely to be uniform in space and time in reality. The model receives a bioavailable supply of aeolian-derived iron of 2.6×10^9 mol Fe yr^{-1}. Below the surface layer, $S_{Fe} = 0$.

[19] The second and third terms on the right of equation (7) represent ocean transport of total iron. Γ is the biological utilization in phosphorus units which is scaled here by the stoichiometric ratio (R_{Fe} = Fe:*P*) for biological processes. Below the euphotic zone, the biological uptake (Γ) is zero. There is a source of Fe_T due to the remineralization of DOM, λDOP R_{Fe}, again assuming fixed stoichiometry. Last, J_{Fe} represents the sink of iron due to scavenging. We assume a fixed stoichiometry, R_{Fe} = 0.47 mmol Fe:mol P, for iron and phosphorus during biological uptake, export, and remineralization (assuming a fixed Fe:C ratio of 4 μmol:1 mol and a *C*:*P* Redfield ratio of 117:1 [*Anderson and Sarmiento*, 1994]). This represents a mean community value which we apply in this model which does not resolve the ecosystem. *Sunda and Huntsman* [1995] show that marine phytoplankton can decrease their cellular iron requirement to optimize growth in Fe-stressed environments, but we have not represented this variability here, as a clear relationship has not been established.

[20] Here dissolved iron is assumed to be the sum of "free" Fe′ and "complexed" *FeL* forms,

$$Fe_T = Fe' + FeL, \tag{9}$$

where *FeL* represents the iron complexed with an organic ligand, *L*. Since the solubility of iron is very low in high-pH, high-temperature surface waters, on the order of 0.011 nM [*Liu and Millero*, 2002], we rapidly precipitate *Fe*′ when $Fe_T > L_T$. It is assumed that only the free form is susceptible to scavenging, and we represent this as a first-order loss process.

$$J_{Fe} = -k_{sc} Fe'. \tag{10}$$

Laboratory and field observations of thorium isotopes indicate that particle concentration also limits scavenging [*Honeyman et al.*, 1988, and references therein]. Compiling oceanic field data, *Honeyman et al.* [1988] fit a power law

Table 1. Model Parameters

Symbol	Definition	Value
β	Fe dust solubility	1%
R_{Fe}	Fe:P ratio	0.47 mmol:1 mol
ν	fraction of DOP	0.67
μ	maximum biological uptake	0.5 μM $month^{-1}$
λ	remineralization rate	0.5 yr^{-1}
K_{Fe}	iron half saturation constant	0.12 nM
K_{PO4}	phosphate half saturation constant	0.5 μM
I_0	light half saturation constant	30 W m^{-2}
τ	scavenging scaling factor	0.2
ϕ	*Honeyman et al.* [1988] exponent coefficient	0.58
k_0	initial Scavenging rate	0.079 L^{ϕ} mg^{ϕ} d^{-1}
W_{sink}	particle sinking rate	2900 m yr^{-1}
$\log(K_{FeL})$	ligand conditional stability constant	11.0

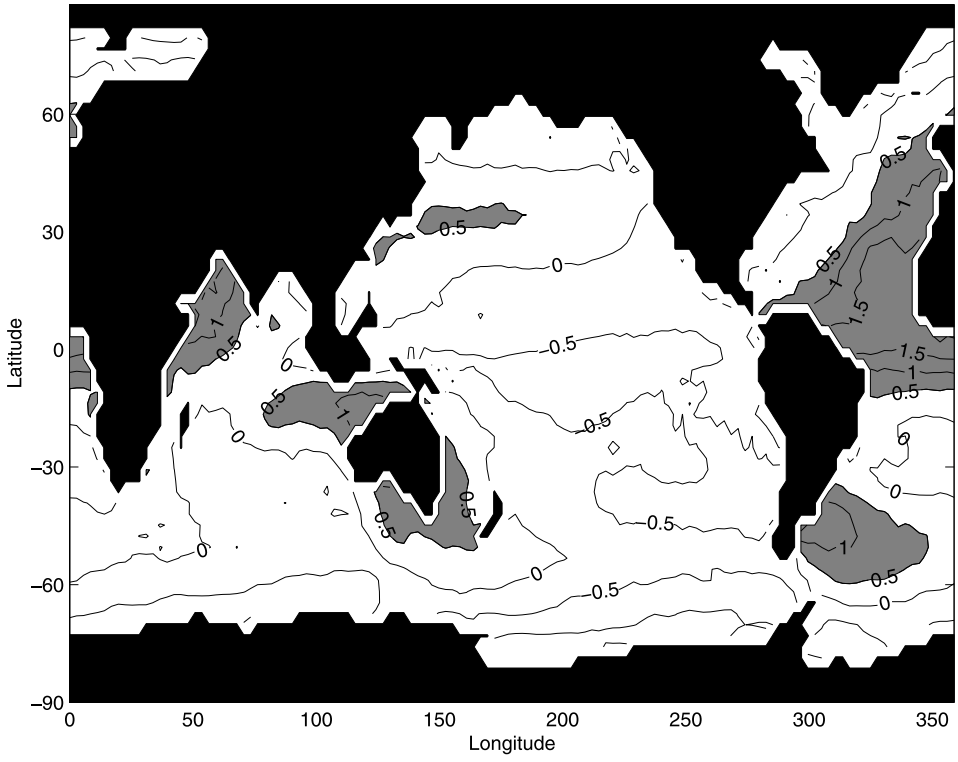

Figure 4. Annually averaged dust deposition (log scale, mg *Fe* m^{-2} yr^{-1}) simulated from an atmospheric model [*Luo et al.*, 2003]. Values greater than log(0.5) are shaded. The model is forced monthly.

function to describe the relationship between scavenging rate (k_{sc}) and particle concentration (C_p), which we apply here,

$$k_{sc} = \tau k_0 C_p^{\phi}, \tag{11}$$

where k_0 represents the scavenging rate when particles are not limiting, C_p is the particle concentration, and ϕ is a constant coefficient. C_p is determined locally from the modeled sinking particle flux and an assumed sinking rate. Thus scavenging is more efficient in the upper water column, i.e., biologically active regions of the ocean. C_p decreases with depth. *Honeyman et al.* [1988] empirically determine k_0 and ϕ. Since the empirical relationship was calculated using thorium, we scale the scavenging rate (τ) by 0.2. With this scaling factor, scavenging rates in surface waters range from 0 to 0.45 yr^{-1} depending on particle concentration. These scavenging rates gave reasonable surface iron concentrations in our box model study [*Parekh et al.*, 2004].

[21] Since complexation occurs on the timescales of minutes to hours [*Witter et al.*, 2000b], it is assumed that the reaction goes to equilibrium. We specify the total ligand concentration, $L_T = [FeL] + [L']$, and use the equilibrium relationship $K_{FeL} = k_f/k_d = [FeL]/[Fe'][L']$ to determine the speciation of the iron. In all the model runs discussed here we set the total ligand concentration, L_T = 1 nM. The assumption of a uniform total ligand concentration is necessary owing to the current lack of understanding of its nature and sources and sinks. This simplification was also used by *Archer and Johnson* [2000] though they chose a lower value (L_T = 0.6 nM). Recent observations suggest higher total ligand concentrations in the ocean, and typically there is excess ligand, over and above that complexed with iron [*Gledhill and van den Berg*, 1994; *Rue and Bruland*, 1995; *van den Berg*, 1995; *Wu and Luther*, 1995; *Rue and Bruland*, 1997; *Gledhill et al.*, 1998; *Nolting et al.*, 1998; *Witter and Luther*, 1998; *Witter et al.*, 2000a; *Boye et al.*, 2001; *Powell and Donat*, 2001]. We impose the conditional stability constant, or ligand strength, $\log(K_{FeL})$ = 11.0, within the range suggested by laboratory and field studies and constrained by the results of sensitivity studies with a box model [*Parekh et al.*, 2004].

3. Modeled Distributions of Iron and Phosphate

[22] The model has been integrated for 3500 years. We considered the model to have reached equilibrium when there was a repeating annual cycle at the surface and very small trends at depth (i.e., when PO_4 changed by less than 0.001 μM over 100 years). Here we discuss the resulting PO_4 and Fe_T distributions.

3.1. Iron

3.1.1. Surface

[23] In qualitative agreement with the observed distribution (Figure 1a), the model predicts elevated surface [Fe_T] in the Atlantic basin and the Indian Ocean (Figure 5a). In both basins, surface [Fe_T] are as high as 1 nM. The modeled concentration does not generally exceed 1 nM because we

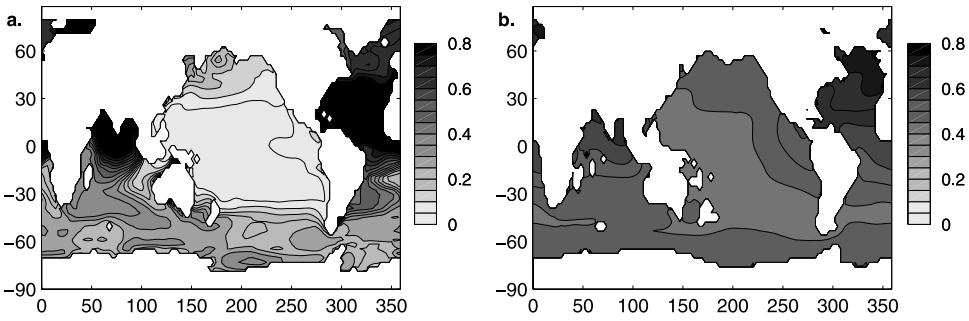

Figure 5. Annually averaged modeled [Fe_T] (nM) at (a) surface and (b) 935 m. See color version of this figure at back of this issue.

have imposed a uniform $L_T = 1$ nM and precipitate Fe' when $Fe_T > L_T$ due to the very low solubility of free iron in high-pH, high-temperature surface waters [*Liu and Millero*, 2002].

[24] Iron concentrations as high as ~0.9 nM have been measured in surface waters of the Sargasso Sea [*Boyle et al.*, 2005] and the southwestern Atlantic [*Vink and Measures*, 2001]. There have been observations of even higher surface concentrations. *Measures and Vink* [1999] observed elevated [Fe_T] in the Arabian Sea, as high as 2.4 nM, in July and August of 1995 and, recently, *Landing et al.* [2004] have measured [Fe_T] in excess of 1.5 nM in Northern Atlantic surface waters. Higher iron concentrations might be expected in Atlantic surface waters owing to the strong local aeolian source from the Sahara desert. In addition, higher ligand concentrations than the 1 nM imposed in the model have been observed, which could sustain higher complexed iron concentrations than are possible in these model runs. It is also likely that high surface *Fe* exists as colloids rather than truly in solution, but in order to separate colloidal and soluble iron, it is necessary to filter samples with a 0.02 μm filter [*Wu and Boyle*, 2002].

[25] The model also predicts higher surface [Fe_T] in the northwestern Pacific relative to the northeastern Pacific, in broad agreement with observations (Figure 1a) and reflecting areas of elevated dust flux (Figure 4). Light limitation during the winter months in the North Pacific basin also contributes to surface Fe_T buildup. In the rest of the Pacific basin, [Fe_T] is close to complete drawdown in the model, which may be too low compared to the few observations. This is attributable to low aeolian input and the upwelling of deep waters with a very high iron deficit. The latter effect may be excessive in this coarse resolution model (see section 3.2).

[26] Surface [Fe_T] is observed in the Pacific sector of the Southern Ocean (Figure 1a) ranging from 0.1 to greater than 0.6 nM in the coastal waters of the Southern Ocean [*Grotti et al.*, 2001]. The model indicates [Fe_T] between 0.15 and 0.35 nM in all sectors of the Southern Ocean. While dust flux is relatively low in this region (Figure 4) and upwelling waters are iron deficient (see section 3.3), light limitation due to ice cover is a significant limiting factor for much of the year in the high-latitude Southern Ocean and prevents complete drawdown of both macronutrients and micronutrients in this model. Hence the annual mean Fe_T remains finite in this region though it may be drawn down in summer. Comparing the fraction of the year over which each nutrient (light, iron, or phosphate) is limiting shows that in the annual mean sense, light is the most dominant limiting factor close to the Antarctic continent in this model.

3.1.2. Mid-Depth Iron Distribution

[27] In Figure 5b we show the modeled Fe_T distribution at 935 m which can be compared with Figure 1b. The modeled distribution is qualitatively consistent with the sparse observations, showing highest [Fe_T] in the North Atlantic basin, ranging between 0.6 and 0.8 nM, decreasing to the south. The North Atlantic values are slightly higher than the current data compilation suggests (Figure 1b), but recent, unpublished, observations [*Landing et al.*, 2004] suggest that thermocline values can significantly exceed 0.8 nM in the region.

[28] The model suggests a gradient of [Fe_T] in the Pacific at these depths, decreasing to the south, which is supported by the sparse observations (Figure 1b). However, with the illustrated set of parameterizations and parameter choices, the model appears to slightly underestimate [Fe_T] in the North Pacific and overpredict [Fe_T] in the Southern Ocean waters. *Martin et al.* [1989] observed elevated [Fe_T] in the Gulf of Alaska owing to the contribution of iron from reducing sediments. Since we do not consider this source, it is to be expected that our model underpredicts [Fe_T] in the North Pacific.

[29] It is pleasing that these basic parameterizations lead to simulations which are at least qualitatively consistent with the observed iron distribution. However, we are very data limited at present. To our knowledge, there are no published measurements of iron in the South Pacific and South Atlantic, making it impossible to assess the performance of such models for these regions at this time.

3.1.3. Vertical Iron Distribution

[30] We compare modeled and observed vertical profiles of iron in the three HNLC regions in Figure 6. Both observed data and model tend to show a sharp increase in the upper thermocline and very uniform mid-depth and deep water concentrations. The model results are generally in reasonable qualitative agreement with the observed data. In particular, in the North Pacific, the model results match reasonably with observations throughout the water column with an offset of about 0.1 nM. In both the equatorial Pacific and Southern Ocean profiles, the data show more

vertical structure than the model with a suggestion of more elevated values in the bottom waters relative to those at mid-depth. This may be partly due to the relatively weak deep water overturning cell and bottom water formation rate in the numerical model or lack of representation of sedimentary sources of iron.

3.1.4. Comparison to Other Models

[31] There are several, previously published models of the global iron cycle, including that of *Aumont et al.* [2003], *Gregg et al.* [2003], and *Archer and Johnson* [2000]. Our surface iron concentrations are qualitatively similar to the model of *Aumont et al.* [2003], with low surface [Fe_T] in the Pacific and higher [Fe_T] in high dust flux regions such as the North Atlantic and Indian Oceans. *Aumont et al.* [2003] do not show deep water [Fe_T]. Since they use the parameterization of *Johnson et al.* [1997], in which [Fe_T] > 0.6 nM is rapidly scavenged, we expect that their model is not able to resolve deep water *Fe* gradients. Our surface distribution of Fe_T also agrees well qualitatively with the model of *Gregg et al.* [2003]. They only ran their model for 26 years, so it is not possible to compare deep water [Fe_T].

[32] The model of *Archer and Johnson* [2000] removes any surface iron from the system that is not utilized biologically. This implies that high [Fe_T] are not found in the surface layer of their model in high dust flux regions such as the North Atlantic, at odds with more recent Fe observations. We compare our model results with *Archer and Johnson*'s [2000] one ligand and two ligand cases at 350 m and 2500 m. We find that their model predicts a fairly uniform distribution of iron which is not in agreement with more recent measurements of iron. We believe our model is able to predict deep water iron gradients because of our choice of an intermediate ligand strength and a greater concentration of total ligand, while *Archer and Johnson* [2000] use a fast scavenging rate and restrict the total ligand concentration to 0.6 nM, forcing the deep iron concentrations toward 0.6 nM.

3.1.5. Supply of New Iron to Surface Waters

[33] We evaluate the relative contribution of iron being supplied from below (considering the advective, implicit diffusion and eddy terms) and aeolian iron to the surface ocean. The upward vertical transport of iron in our model is 1.7×10^9 mol *Fe* yr^{-1}, lower than the estimate of *Aumont et al.* [2003] of 3.65×10^9 mol *Fe* yr^{-1}, but higher than the data-based estimate of *Fung et al.* [2000] of 0.7×10^9 mol *Fe* yr^{-1}. HAMOCC5, the three-dimensional general circulation model used by *Aumont et al.* [2003] has stronger convective adjustment than the MITGCM [*Dutay et al.*, 2002] which can partially explain why HAMOCC5 predicts a larger upward vertical transport. Additionally, *Aumont et al.* [2003] force deep water [Fe_T] toward 0.6 nM, a higher concentration than has been measured in certain regions of the ocean such as the Southern Ocean. As argued by *Aumont et al.* [2003], we believe our estimate for upward vertical transport is much higher than the data-based estimate of *Fung et al.* [2000] because of convective mixing, whereas *Fung et al.* [2000] only apply a vertical diffusivity coefficient that is never higher than 1 $cm^2\ s^{-1}$.

[34] Assuming that aeolian Fe input (1% bioavailability) and upward vertical transport are the only source of "new" iron to the top 120 m of the model, we calculate that upward vertical transport can account for 40% of the supply to the euphotic zone globally. In the Southern Ocean, 83% of iron to the euphotic zone is supplied by vertical transport. *Aumont et al.* [2003] predict that 70% of new iron is derived from below. In addition to the HAMOCC5 model predicting a larger upward supply of iron from below to the euphotic zone, *Aumont et al.* [2003] force their model with less dust annually than our model (1.5×10^9 mol *Fe* yr^{-1} compared to 2.6×10^9 mol *Fe* yr^{-1}), resulting in a much larger contribution of new iron from below. Alternatively, *Fung et al.* [2000] also predict ~40% of iron to be supplied by upward vertical transport globally, assuming 1% bioavailability of aeolian-derived Fe. While the estimates of fraction of new iron vary widely, between 40 and 70%, it is clear that upwelling is an important source of iron to the euphotic zone.

3.2. Phosphate

[35] Figure 7 illustrates the modeled phosphate distribution compared to global PO_4 maps [*Conkright et al.*, 2002]. The model captures the broad pattern of the observed phosphate distribution, most notably elevated surface [PO_4] in the so-called HNLC regions of the Southern Ocean, tropical Pacific, and subarctic Pacific. This is a consequence of explicit iron limitation in this model and does not require any artificial regional variation in the maximum export rate, as was used by *McKinley et al.* [2003, 2004] or restoration toward observed surface macronutrient concentrations [e.g., *Najjar et al.*, 1992].

[36] In the North Pacific, the model slightly underestimates the surface [PO_4]. The high PO_4 tongue in the low-latitude Pacific is slightly misplaced in the model, and modeled surface subtropical [PO_4] is generally too high in the model. Since Fe_T is fully drawn down in that region, it is clear that the model is iron limited there. This feature is robust across a range of model parameters and may be attributable to the coarse resolution configuration of the model. Ocean GCMs at such coarse resolution do not resolve important equatorial dynamical processes, including the undercurrents, resulting in erroneous upwelling of deep Pacific waters directly to the surface. *Aumont et al.* [1999] demonstrated that this lack of resolution could lead to "nutrient trapping" in such models with surface nutrient restoring [*Najjar et al.*, 1992]. Here it leads to an excessive supply of phosphate rich, strongly iron depleted waters from the subsurface Pacific directly to the surface. The tropics are too iron limited, and the elevated PO_4 brought to the surface by upwelling is advected laterally into the surrounding subtropics. Other possible causes include an underestimation of the dust forcing and/or bioavailability of aeolian-derived iron in the model. Recent field results for the eastern North Pacific from *Johnson et al.* [2003] suggest that between 20 and 80% of iron aeolian flux must have been soluble in seawater between March to May 2001 in order to support the observed increase in surface [Fe_T]. *Christian et al.* [2002], adding a scavenging based iron cycle model to a three-dimensional, physical biogeochemical model of the tropical Pacific Ocean, also find that their model wrongly suggests iron limitation in the western Pacific. They suggest

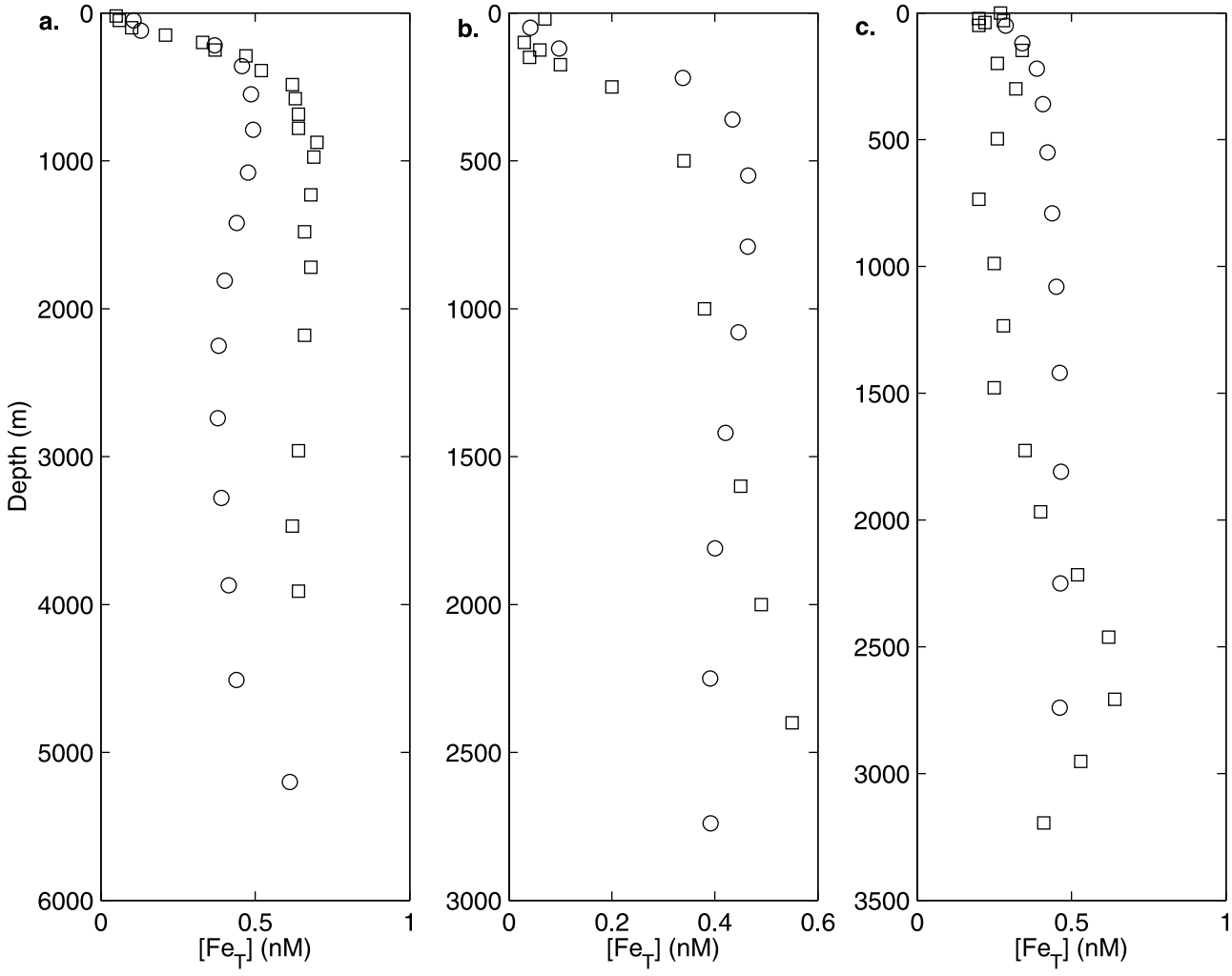

Figure 6. Comparison of modeled (circles) and observed (squares) *Fe* profiles in HNLC regions. (a) North Pacific: 50°N, 145°W [*Martin et al.*, 1989]. (b) Equatorial Pacific: 3°S, 140°W [*Coale et al.*, 1996b]. (c) Southern Ocean: 56°S, 143.4°E [*Sohrin et al.*, 2000].

that the equatorial undercurrent may be transporting iron from hydrothermal sources to surface waters in this region, and this is not represented in the models. Additionally, reducing ocean margin sediments may serve as a source for iron, which is also not represented in our model.

3.3. *Fe**: A Tracer of Iron Limitation

[37] The scavenging of iron from the water column results in the decoupling of *Fe* and PO_4. Regions where upwelled waters are highly deficient in *Fe* require a high aeolian *Fe* flux to compensate; otherwise iron limitation occurs. Here we construct a tracer which tracks the relative magnitude of decoupling between *Fe* and PO_4. Similar to *N** [*Gruber and Sarmiento*, 1997], we subtract the contribution of the soft tissue pump from the Fe_T distribution to reveal the balance between physical transport and scavenging of iron. We define

$$Fe^* = Fe_T - R_{Fe}PO_4. \quad (12)$$

The governing equation for *Fe** is

$$\frac{\partial Fe^*}{\partial t} = \beta F_{in} - \bigtriangledown \cdot (\mathbf{u}Fe^*) + \bigtriangledown \cdot (\kappa \bigtriangledown Fe^*) - k_{sc}Fe. \quad (13)$$

By removing the soft tissue pump contribution, *Fe** reveals the balance between advected and scavenged iron. (It is important to note that we must know R_{Fe}, the biological ratio of *Fe*:PO_4, to evaluate *Fe**. In nature, *Fe*:PO_4 and *Fe*:*C* are not likely to be constant [*Sunda and Huntsman*, 1995], but in the model we have imposed a fixed biological *Fe*:*P* ratio of 0.47 mmol:1 mol. Hence *Fe** can be a useful diagnostic of the model.) In the model, positive *Fe** implies adequate *Fe* to support the complete biological utilization of PO_4, while a negative *Fe** means that there is a deficit in *Fe*.

[38] Figure 8a shows zonally averaged *Fe** in the Atlantic basin of the model, revealing the regions of iron deficit. In the North Atlantic, where aeolian input is high, *Fe** is positive at all depths. This signature of the strong aeolian deposition is carried to the deep waters by the western

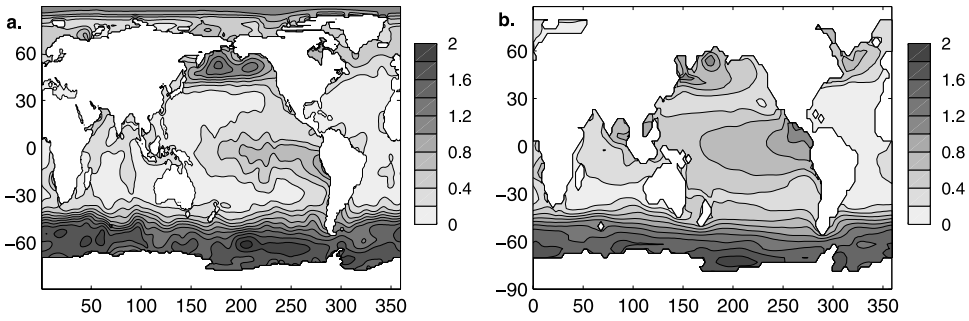

Figure 7. Annually averaged surface PO_4 (μM): (a) Climatology [*Conkright et al.*, 2002] and (b) model results. See color version of this figure at back of this issue.

boundary current and southward by North Atlantic Deep Water to approximately 35°S. Farther south, scavenging has depleted the excess Fe to the point that it is now limiting. The gradual decrease in *Fe** from north to south implies a fairly long residence time for dissolved iron in the ocean model. The global mean ocean residence time for iron is 233 years in the model. (Mean yearly soluble aeolian supply in the model is 2.6×10^9 mol *Fe* yr^{-1}, and the global ocean loading of iron is 6.06×10^{11} mol *Fe*).

[39] In the Indo-Pacific basin *Fe** is negative everywhere (Figure 8b) except in the surface waters of the Indian basin, and the iron deficit is greatest in deep Northern Pacific waters. Since these are the oldest waters in the ocean, the iron has been stripped away by scavenging, while PO_4 has been accumulating, resulting in the strongest decoupling anywhere in the domain. Thus, despite the fact that dust deposition is relatively high in the North Pacific, HNLC conditions are still prevalent, as the aeolian-derived *Fe* is not enough to compensate for the very low *Fe** in the upwelling waters.

4. Sensitivity Studies

[40] The model results reflect only a single solution of the circulation and biogeochemistry model in which the choice of parameter values was guided by information from laboratory and field studies. However, some of these parameters are not well constrained, and we have also used an extensive suite of sensitivity experiments with a computationally efficient model to guide these parameter choices [*Parekh et al.*, 2004]. In this section we use the more complex circulation and biogeochemistry model to explore the sensitivities of modeled Fe_T and PO_4 to changes in the efficiency of scavenging of iron as well as the model's physical forcing and circulation. Even at this relatively coarse resolution, only a limited number of global, equilibrium spin-ups are viable, and so we present the results of two focused studies. We use them to examine whether the sensitivities suggested by the box model [*Parekh et al.*, 2004] are robust in this more sophisticated (and perhaps more realistic) framework. Sensitivity studies are integrated for 1000 years.

4.1. Scavenging and Complexation

[41] Our previous box model studies [*Parekh et al.*, 2004] suggested that the basin to basin gradients of iron in the deep ocean are critically controlled by the ratio of the conditional stability coefficient, to the scavenging rate, K_{FeL}/k_{sc}. Increasing this ratio enhances the protection of dissolved iron from scavenging by binding iron more

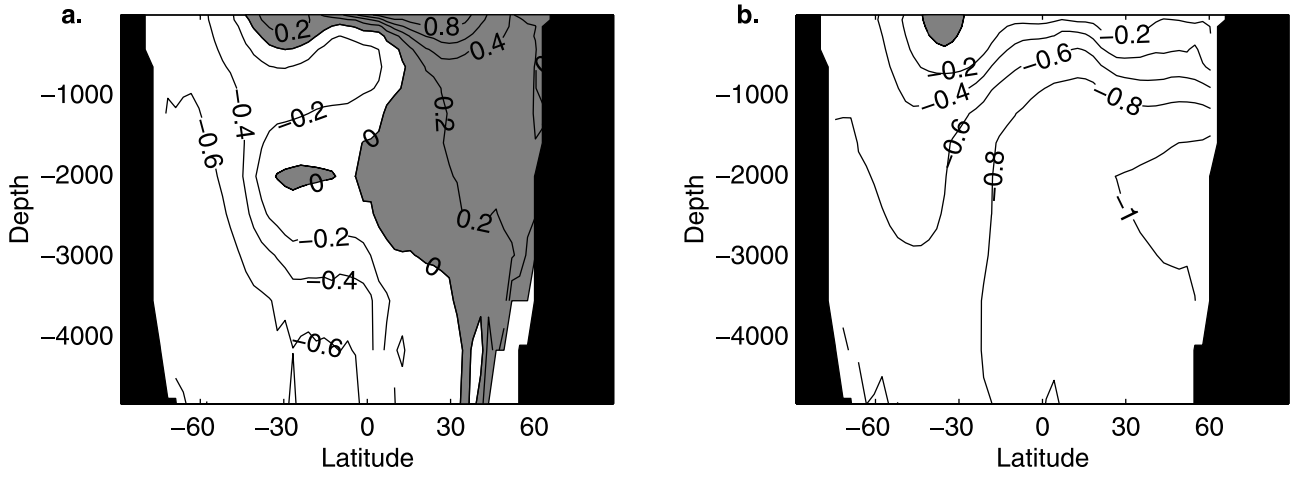

Figure 8. Zonally averaged section of *Fe** in the (a) Atlantic basin and (b) Indo-Pacific basin. In shaded regions, *Fe** is greater than zero.

strongly to the organic ligand. The conditional stability coefficient, K_{FeL}, and scavenging rate, k_{sc}, are somewhat constrained from laboratory and field studies and by analogy to thorium, respectively. However, the uncertainties allow a range of several orders of magnitude. The ratio imposed in the general circulation and biogeochemical model was guided by the suite of box model sensitivity studies [*Parekh et al.*, 2004] selecting a value which best captured the observed basin to basin gradients of deep dissolved iron in that case. It is pleasing that this initial choice of the ratio results in good qualitative agreement between model and observations. Is the iron distribution sensitive to this parameter in the GCM? If so, is its sensitivity consistent with that of the box model?

[42] Here we illustrate the sensitivity to the ratio K_{FeL}/k_{sc} by decreasing the scavenging rate, k_{sc}, by approximately 40%, to a maximum scavenging rate of 0.27 yr^{-1}. In Figure 9 we illustrate the change in surface PO_4, surface and 935-m Fe_T, and Fe^* at the base of the mixed layer ($\sim$360 m). The resulting changes are qualitatively and quantitatively consistent with the box model studies [*Parekh et al.*, 2004; Figure 7] showing an increase in the deep [Fe_T] (Figure 9c) in all basins on the order of 0.1 nM. The associated increase in the iron concentration in the upwelling waters of the Southern Ocean, as measured by a higher Fe^* in the subsurface waters (Figure 9d), leads to a partial relief of the iron limitation of the model's Southern Ocean. However, there is a significant role of light limitation in that region of the model, enhanced by ice cover, so the difference in Southern Ocean surface PO_4 (Figure 9a) between the two experiments is small (about 5%) relative to the 40% change in scavenging coefficient and the change in deep water iron concentration ($\sim$25% in the Southern Ocean).

[43] The sensitivity of the model to K_{FeL}/k_{sc} can be qualitatively and quantitatively understood from the idealized box model experiments. Increasing K_{FeL}/k_{sc} increases [Fe_T] throughout the model domain and partially relieves iron stress in the Southern Ocean. However, colimitation by light in that regions means that there is only a weak impact on surface PO_4 suggesting a relatively weak dependence of the biological carbon pump on this parameter.

4.2. Circulation and Physical Forcing

[44] Of particular interest with regard to global change is the sensitivity of the iron model and iron limitation of the Southern Ocean to ocean circulation. Here we describe a sensitivity study of the oceanic iron cycle to changes in wind stress forcing. Climate models configured for the Last Glacial Maximum (LGM) have suggested changes in surface stress forcing in the Southern Ocean, consistent with changes in the residual overturning circulation in the region. There is not a clear consensus, however, on the nature of the change. For example, the coupled climate model of *Kim et al.* [2003] suggests weaker wind stress in the Southern Ocean during the LGM and significant changes in the volume flux of circumpolar deep waters reaching the surface. In contrast, in an atmospheric model, with either prescribed sea surface temperatures or a slab ocean mixed-layer model, *Dong and Valdes* [1998] find that winds over the Southern Hemisphere high latitudes change very little. Model results from the Paleoclimate Modeling Intercomparison Project do not agree on whether winds increased or decreased during the LGM relative to modern winds [*Braconnot*, 2000].

[45] It is difficult to separate the effects of wind stress and buoyancy forcing on the Southern Ocean residual overturning circulation [e.g., *Karsten and Marshall*, 2002]. However, in the numerical model we may vary these forcing fields somewhat independently. Here we compare the biogeochemical implications of changes in the imposed wind stress forcing. In the "control" model, illustrated above, we applied *Trenberth et al.* [1989] wind stresses. Here, in a second experiment, the wind stress forcing on the physical model is that of the *Hellerman and Rosenstein* [1983] climatology. While both climatologies are relevant to the atmosphere of the late twentieth century, the latter data set has notably weaker surface wind stresses in the remote Southern Hemisphere, relative to the former, perhaps due to the sparsity of data in the remote Southern Hemisphere at the time it was compiled. (The configuration with *Hellerman and Rosenstein* [1983] winds is actually that used for the OCMIP comparison [e.g., *Dutay et al.*, 2002]). We illustrate the impact of this change in the wind stress forcing on the residual mean overturning circulation of the model in Figure 10. At high southern latitudes it becomes very weak; Ekman and eddy induced flow almost exactly balance in this case. In contrast, the Southern Ocean residual overturning in the control case is relatively strong: about 10 Sv.

[46] Here we examine the response of the coupled ocean phosphorus and iron cycles to this change in the physical forcing and circulation of the model when all biogeochemical parameterizations and boundary conditions are identical. Weakening Southern Ocean overturning circulation leads to a decrease in surface [PO_4] and [Fe_T] in the region (Figures 11a and 11b) due to a reduction in the upwelling strength. The amount of Fe_T and PO_4 upwelled in the Southern Ocean decreases by 33% in this simulation. There is little difference in Fe^* of upwelled waters between the perturbation and the control run (Figure 11d). However, the aeolian source has not changed and now can more significantly affect surface PO_4.

[47] This result suggests that a glacial world with stronger winds would require a major increase in aeolian-derived Fe to increase the effectiveness of the biological pump in order to reduce surface PO_4. If, on the other hand, glacial wind stress forcing was weaker, large increases in the external input of iron are not necessary to draw down surface PO_4. This simplified view omits, of course, many other potential influences on ocean circulation, stratification, and export production which would likely occur in concert and which, as suggested by the model of *Bopp et al.* [2003], may also be significant.

[48] The sign of the sensitivity of the GCM is consistent with that of the simplified box model when using the same scavenging-complexation parameterization of ocean iron biogeochemistry [*Parekh et al.*, 2004] (Figure 11c). It is interesting to note that in the box model the sensitivity to the overturning circulation was of opposite sign when a

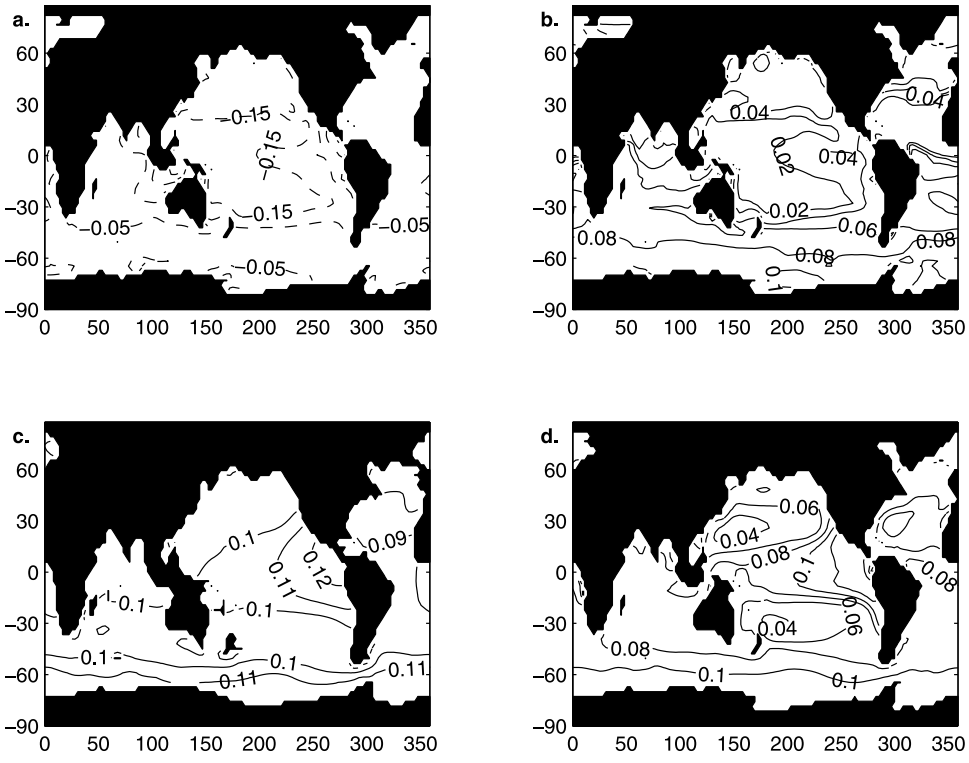

Figure 9. Sensitivity to weaker scavenging rate. Change in (a) surface $[PO_4]$ (μM), (b) surface $[Fe_T]$ (nM), (c) 935 m $[Fe_T]$ (nM), and (d) Fe^* at the base of the mixed layer (360 m). Results presented as perturbation-control run. Dashed contours represent negative values.

simpler, scavenging-desorption iron parameterization (without representation of complexation) was used. This suggests that the form of parameterization can have very important implications for glacial-interglacial simulations.

5. Summary and Discussion

[49] Iron and phosphorus are strongly decoupled in the interior of the ocean owing, at least in part, to the processes of scavenging and complexation with organic ligands which impact only iron. Guided by our previous studies with a highly idealized box model, we have implemented a model of the coupled cycles of phosphorus and iron in the ocean in a general circulation model. We have demonstrated that the model, using parameter values guided by laboratory and field studies along with our simplified box model, qualitatively captures the surface distributions and basin to basin deep gradients of both nutrients. Regions of elevated surface phosphate concentrations arise naturally in the model as a consequence of explicit iron limitation (along with light limitation in the Southern Ocean). More quantitative comparisons of model and data are also favorable, though the present sparsity of oceanic iron observations is clearly a limiting factor.

[50] Sensitivity studies with the three-dimensional model show that its response to changes in scavenging or complexation efficiency and circulation are consistent with, and support the inferences from, the idealized box model studies [*Parekh et al.*, 2004]. The sensitivity to changes in circulation suggests that an increase in wind stress forcing on the Southern Ocean might counteract an increase in the biological pump due to enhanced dust supply to the Southern Ocean in glacial periods. The sign of this sensitivity is, however, critically dependent upon the complexation mechanism.

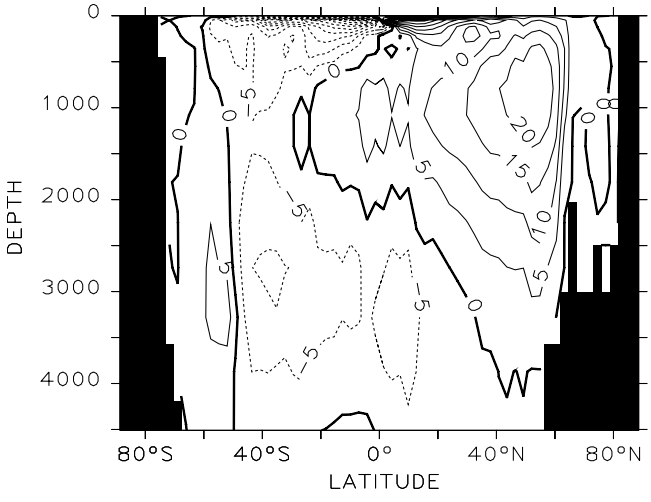

Figure 10. Global residual mean of the model forced with *Hellerman and Rosenstein* [1983] winds. Fluxes are in Sv (10^6 m^3 s^{-1}).

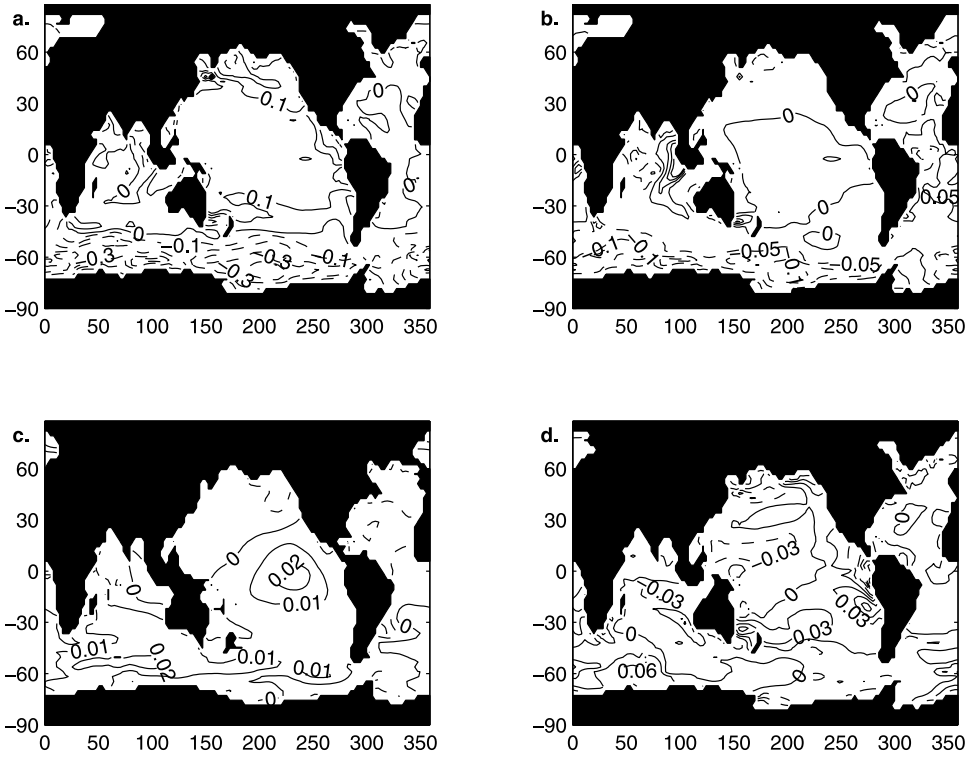

Figure 11. Sensitivity to weaker winds. Change in (a) surface $[PO_4]$ (μM), (b) surface $[Fe_T]$ (nM), (c) 935 m $[Fe_T]$ (nM), and (d) Fe^* at the base of the mixed layer (360 m). Results presented as perturbation-control run. Dashed contours represent negative values.

[51] At this point, we suggest that further progress in modeling the iron cycle, its response to global change, and the implications for the global biogeochemical cycles of other nutrients and carbon is currently limited by the availability of iron observations. We strongly support efforts to provide a global, calibrated survey of the oceanic iron distribution. In addition, the apparent importance of the organic ligands in regulating the iron distribution suggests that we may need dynamic representations of their sources and sinks. This will not be possible until a more detailed understanding emerges from continued field and laboratory studies. A clearer qualitative and quantitative understanding of the controls on the solubility or bioavailability of aeolian iron is also of particular importance. Iron has been implicated as a key micronutrient in ocean biogeochemical cycles and their coupling to the climate system. However, there is still a considerable gap to bridge between the understanding of the basic controls on oceanic iron, our ability to quantitatively parameterize them, and the application of iron cycle models to these fascinating feedbacks and the hypotheses around them.

Appendix A

[52] The following were referenced for the data set used to plot Figure 1: *Blain et al.* [2001], *Boyd et al.* [2000], *Bowie et al.* [2001, 2002], *Boye et al.* [2001, 2003], *Boyle et al.* [2005], *Bruland et al.* [1994], *Bucciarelli et al.* [2001], *Coale et al.* [1996b], P. L. Croot et al., Where does all the iron go? Uncovering the fate of the added iron during the EISENEX iron enrichment experiment, submitted to *Marine Chemistry*, 2005, *de Baar et al.* [1995, 1999], *de Jong et al.* [1998], *Fitzwater et al.* [1996, 2000], *Gledhill and van den Berg* [1994], *Gordon et al.* [1982, 1998], *Grotti et al.* [2001], *Hall and Safi* [2001], *Johnson et al.* [1997, 2001, 2003], *Kuma et al.* [1996, 1998, 2003], *Laes et al.* [2003], *Landing and Bruland* [1987], *Loscher et al.* [1997], *Mackey et al.* [2002], *Martin and Gordon* [1988], *Martin et al.* [1989, 1990, 1993], *Measures and Vink* [1999, 2001], *Nakabayashi et al.* [2001, 2002], *Nishioka et al.* [2001, 2003], *Rue and Bruland* [1995, 1997], *Sarthou et al.* [2003], *Sedwick and DiTullio* [1997], *Sedwick et al.* [1997, 1999, 2000], *Sohrin et al.* [2000], *Takata et al.* [2004], *Takeda et al.* [1995], *Takeda and Obata* [1995], *Timmermans et al.* [2001], *Tsuda et al.* [2003], *Vink and Measures* [2001], *Witter and Luther* [1998], *Witter et al.* [2000a], *Wu and Luther* [1994, 1996], *Wu et al.* [2001], *Wu and Boyle* [2002]. The annotated and fully referenced data set is available for downloading at ocean.mit.edu/mick/Downloads.html.

[53] **Acknowledgments.** P. P. is grateful to the NASA Earth System Science Fellowship (NGT5-30362) for funding. M. J. F. is grateful for funding through the Paradigm NOPP (N000014-02-1-0370) and NSF (OCE-336839). We thank Natalie Mahowald for providing the dust forcing fields and William Landing for making unpublished data available to us. We thank Chris Hill for C.P.U. time on the MIT GCM cluster and Stephanie Dutkiewicz for improvements in the physical model. This paper benefited from fruitful discussions with Stephanie Dutkiewicz and Taka Ito. We thank two anonymous reviewers for their constructive comments.

References

Adcroft, A., C. Hill, and J. Marshall (1997), Representation of topography by shaved cells in a height coordinate ocean model, *Mon. Weather Rev.*, *125*, 2293–2315.

Anderson, L., and J. Sarmiento (1994), Redfield ratios of remineralization determined by nutrient data analysis, *Global Biogeochem. Cycles*, *8*, 65–80.

Archer, D., and K. Johnson (2000), A model of the iron cycle in the ocean, *Global Biogeochem. Cycles*, *14*, 269–279.

Aumont, O., J. Orr, P. Monfray, G. Madec, and E. Maier-Reimer (1999), Nutrient trapping in the equatorial Pacific: The ocean circulation solution, *Global Biogeochem. Cycles*, *13*, 351–369.

Aumont, O., E. Maier-Reimer, S. Blain, and P. Monfray (2003), An ecosystem model of the global ocean including Fe, Si, P colimitations, *Global Biogeochem. Cycles*, *17*(2), 1060, doi:10.1029/2001GB001745.

Blain, S., et al. (2001), A biogeochemical study of the island mass effect in the context of the iron hypothesis: Kerguelen Islands, Southern Ocean, *Deep Sea Res., Part I*, *48*, 163–187.

Bopp, L., K. Kohfeld, and C. L. Quéré (2003), Dust impact on marine biota and atmospheric CO_2, *Paleoceanography*, *18*(2), 1046, doi:10.1029/2002PA000810.

Bowie, A., M. Maldonado, R. Frew, P. L. Croot, E. P. Achterberg, R. F. C. Mantoura, P. J. Worsfold, C. S. Law, and P. W. Boyd (2001), The fate of added iron during a mesoscale fertilisation experiment in the Southern Ocean, *Deep Sea Res., Part II*, *48*, 2703–2743.

Bowie, A., D. Whitworth, E. Achterberg, R. F. C. Mantoura, and P. Worsfold (2002), Biogeochemistry of Fe and other trace elements (Al, Co, Ni) in the upper Atlantic Ocean, *Deep Sea. Res., Part I*, *49*, 605–636.

Boyd, P., et al. (2000), A mesoscale phytoplankton bloom in the polar Southern Ocean stimulated by iron fertilization, *Nature*, *407*, 695–702.

Boyd, P., et al. (2004), The decline and fate of an iron-induced subarctic phytoplankton bloom, *Nature*, *428*, 549–553.

Boye, M., C. van den Berg, J. de Jong, H. Leach, P. Croot, and H. de Baar (2001), Organic complexation of iron in the Southern Ocean, *Deep Sea Res., Part I*, *48*, 1477–1497.

Boye, M., A. Adrich, C. van den Berg, J. deJong, M. Veldhuis, and H. de Baar (2003), Horizontal gradient of the chemical speciation of iron in surface waters of the northeast Atlantic Ocean, *Mar. Chem.*, *80*, 129–143.

Boyle, E., B. Bergquist, R. Kayser, and N. Mahowald (2005), Iron, manganese and lead at Hawaii Ocean Time-series Station ALOHA: Temporal variability and an intermediate water hydrothermal plume, *Geochem. Cosmochim. Acta*, *69*, 933–952.

Braconnot, P. (2000), Paleoclimate Modeling Intercomparison Project (PMIP): Proceedings of the Third PMIP Workshop, *WCRP-111*, 271 pp., World Clim. Res. Program, Geneva.

Bruland, K. W., K. J. Orians, and J. P. Cowen (1994), Reactive trace metals in the stratified central North Pacific, *Geochem. Cosmochim. Acta*, *58*, 3171–3182.

Bucciarelli, E., S. Blain, and P. Treguer (2001), Iron and manganese in the wake of the Kerguelen Islands (Southern Ocean), *Mar. Chem.*, *73*, 21–36.

Buesseler, K., J. Andrews, S. Pike, and M. Charette (2004), The effects of iron fertilization on carbon sequestration in the Southern Ocean, *Science*, *304*, 414–417.

Charette, M., and K. Buesseler (2000), Does iron fertilization lead to rapid carbon export in the Southern Ocean?, *Geochem. Geophys. Geosyst.*, *1*, doi:10.1029/2000GC000069.

Christian, J., M. Verschell, R. Murtugudde, A. Busalacchi, and C. McClain (2002), Biogeochemical modelling of the tropical Pacific Ocean: II. Iron biogeochemistry, *Deep Sea Res., Part II*, *49*, 545–565.

Coale, K., et al. (1996a), A massive phytoplankton bloom induced by an ecosystem-scale iron fertilization experiment in the equatorial Pacific Ocean, *Nature*, *383*, 495–501.

Coale, K., S. Fitzwater, R. Gordon, K. Johnson, and R. Barber (1996b), Control of community growth and export production by upwelled iron in the equatorial Pacific Ocean, *Nature*, *379*, 621–624.

Coale, K., et al. (2004), Southern Ocean iron enrichment experiment: Carbon cycling in high- and low-Si waters, *Science*, *304*, 408–414.

Conkright, M., H. E. Garcia, T. D. O'Brien, R. A. Locarnini, T. P. Boyer, C. Stephens, and J. I. Antonov (2002), *World Ocean Atlas 2001*, vol. 4, *Nutrients*, *NOAA Atlas NESDIS 52*, Natl. Oceanic and Atmos. Admin., Silver Spring, Md.

de Baar, H. J. W., and J. T. M. de Jong (2001), Distributions, sources and sinks of iron in seawater, in *The Biogeochemistry of Iron in Seawater*, 1st ed., edited by D. R. Turner and K. A. Hunter, pp. 123–253, John Wiley, Hoboken, N. J.

de Baar, H., J. de Jong, D. Bakker, B. Loscher, C. Veth, U. Bathmann, and V. Smetacek (1995), Importance of iron for plankton blooms and carbon dioxide drawdown in the Southern Ocean, *Nature*, *373*, 412–415.

de Baar, H. J., J. T. de Jong, R. F. Nolting, K. R. Timmermans, M. A. van Leeuwe, U. Bathmann, M. R. van der Loeff, and J. Sildam (1999), Low dissolved Fe and the absence of diatom blooms in remote Pacific waters of the Southern Ocean, *Mar. Chem.*, *66*, 1–34.

de Jong, J., J. den Das, U. Bathmann, M. Stoll, G. Kattner, R. Nolting, and H. de Baar (1998), Dissolved iron at subnanomolar levels in the Southern Ocean as determined by ship-board analysis, *Anal. Chim. Acta*, *377*, 113–124.

Doney, S., et al. (2004), Evaluating global ocean carbon models: The importance of realistic physics, *Global Biogeochem. Cycles*, *18*, GB3017, doi:10.1029/2003GB002150.

Dong, B., and P. Valdes (1998), Simulations of the Last Glacial Maximum climates using a general circulation model: Prescribed versus computed sea surface temperatures, *Clim. Dyn.*, *14*, 571–591.

Duce, R., and N. Tindale (1991), Atmospheric transport of iron and its deposition in the ocean, *Limnol. Oceanogr.*, *36*, 1715–1726.

Dutay, J.-C., et al. (2002), Evaluation of ocean model ventilation with CFC-11: Comparison of 13 global ocean models, *Ocean Modell.*, *4*, 89–120.

Elrod, V. A., W. M. Berelson, K. H. Coale, and K. S. Johnson (2004), The flux of iron from continental shelf sediments: A missing source for global budgets, *Geophys. Res. Lett.*, *31*, L12307, doi:10.1029/2004GL020216.

Falkowski, P. (1997), Evolution of the nitrogen cycle and its influence on the biological sequestration of CO_2 in the ocean, *Nature*, *387*, 272–275.

Fitzwater, S., K. Coale, R. Gordon, K. Johnson, and M. Ondrusek (1996), Iron deficiency and phytoplankton growth in the equatorial Pacific, *Deep Sea Res., Part II*, *43*, 995–1015.

Fitzwater, S., K. Johnson, R. Gordon, and K. C. W. Smith (2000), Trace metal concentration in the Ross Sea and their relationship with nutrients and phytoplankton growth, *Deep Sea Res., Part II*, *47*, 3159–3179.

Fung, I., S. Meyn, I. Tegen, S. Doney, J. John, and J. Bishop (2000), Iron supply and fixation in the upper ocean, *Global Biogeochem. Cycles*, *14*, 281–295.

Gao, Y., Y. Kaufman, D. Tanre, D. Kolber, and P. Falkowski (2001), Seasonal distribution of aeolian iron fluxes to the global ocean, *Geophys. Res. Lett.*, *28*, 29–32.

Gent, P., and J. McWilliams (1990), Isopycnal mixing in ocean circulation models, *J. Phys. Oceanogr.*, *22*, 625–651.

Gledhill, M., and C. van den Berg (1994), Determination of complexation of iron(III) with natural organic complexing ligands in seawater using cathodic stripping voltammetry, *Mar. Chem.*, *47*, 41–54.

Gledhill, M., C. van den Berg, R. Nolting, and K. Timmermans (1998), Variability in the speciation of iron in the northern North Sea, *Mar. Chem.*, *59*, 283–300.

Gordon, R., J. Martin, and G. Knauer (1982), Iron in north-east Pacific waters, *Nature*, *299*, 611–612.

Gordon, R., K. S. Johnson, and K. H. Coale (1998), The behavior of iron and other trace elements during the IronEx I and PlumEx experiments in the equatorial Pacific, *Deep Sea Res., Part II*, *45*, 995–1041.

Gregg, W., P. Ginoux, P. Schopf, and N. Casey (2003), Phytoplankton and iron: Validation of a global three-dimensional ocean biogeochemical model, *Deep Sea Res., Part II*, *50*, 3143–3169.

Grotti, M., F. Soggia, M. Abelmoschi, P. Rivoar, E. Magi, and R. Frache (2001), Temporal distribution of trace metals in Antarctic coastal waters, *Mar. Chem.*, *76*, 189–209.

Gruber, N., and J. Sarmiento (1997), Global patterns of marine nitrogen fixation and denitrification, *Global Biogeochem. Cycles*, *11*, 235–266.

Hall, J., and K. Safi (2001), The impact of in situ Fe fertilisation on the microbial food web in the Southern Ocean, *Deep Sea Res., Part II*, *48*, 2591–2613.

Hellerman, S., and M. Rosenstein (1983), Normal monthly wind stress over the world ocean with error estimates, *J. Phys. Oceanogr.*, *13*, 1093–1104.

Honeyman, B., and P. Santschi (1989), A Brownian-pumping model for trace metal scavenging: Evidence from Th isotopes, *J. Mar. Res.*, *47*, 951–992.

Honeyman, B., L. Balistrieri, and J. Murray (1988), Oceanic trace metal scavenging and the importance of particle concentration, *Deep Sea Res., Part I*, *35*, 227–246.

Hutchins, D., and K. Bruland (1998), Iron-limited diatom growth and Si:N uptake ratios in a coastal upwelling regime, *Nature*, *393*, 561–564.

Ito, T., M. Follows, and J. Marshall (2004), What controls the uptake of transient tracers in the Southern Ocean?, *Global Biogeochem. Cycles*, *18*, GB2021, doi:10.1029/2003GB002103.

Jickells, T. D., and L. Spokes (2001), Atmospheric iron inputs to the oceans, in *The Biogeochemistry of Iron in Seawater*, 1st ed., edited by D. R. Turner and K. A. Hunter, pp. 85–121, John Wiley, Hoboken, N. J.

Johnson, K., R. Gordon, and K. Coale (1997), What controls dissolved iron concentrations in the world ocean?, *Mar. Chem.*, *57*, 137–161.
Johnson, K., F. Chavez, and G. Friederich (1999), Continental-shelf sediment as a primary source of iron for coastal phytoplankton, *Nature*, *398*, 697–699.
Johnson, K., V. Elrod, J. Nowicki, K. Coale, and H. Zamzow (2000), Continuous flow techniques for on site and in situ measurements of metals and nutrients in sea water, in *In Situ Monitoring of Aquatic Systems*, edited by J. Bulle and G. Horvai, pp. 223–252, John Wiley, Hoboken, N. J.
Johnson, K., F. Chavez, V. Elrod, S. Fitzwater, J. Pennington, K. Buck, and P. Walz (2001), The annual cycle of iron and the biological response in central California coastal waters, *Geophys. Res. Lett.*, *28*, 1247–1250.
Johnson, K., et al. (2003), Surface ocean–lower atmosphere interactions in the northeast Pacific Ocean gyre: Aerosols, iron, and the ecosystem response, *Global Biogeochem. Cycles*, *17*(2), 1063, doi:10.1029/2002GB002004.
Karl, D., A. Michaels, B. Bergman, D. Capone, E. Carpenter, R. Letelier, F. Lipschultz, H. Paerl, and D. Sigman (2002), Dinitrogen fixation in the world's oceans, *Biogeochemistry*, *57/58*, 47–98.
Karsten, R., and J. Marshall (2002), Constructing the residual circulation of the ACC from observations, *J. Phys. Oceanogr.*, *32*, 3315–3327.
Kim, S.-J., G. Flato, and G. Boer (2003), A coupled climate model simulation of the Last Glacial Maximum: 2. Approach to equilibrium, *Clim. Dyn.*, *20*, 635–661.
Kuma, K., J. Nishioka, and K. Matsunaga (1996), Controls on iron (III) hydroxide solubility in seawater: The influence of pH and natural organic chelators, *Limnol. Oceanogr.*, *41*, 396–407.
Kuma, K., A. Katsumoto, H. Kawakami, F. Takatori, and K. Matsunaga (1998), Spatial variability of Fe(III) hydroxide solubility in the water column of the northern North Pacific Ocean, *Deep Sea Res., Part I*, *45*, 91–113.
Kuma, K., Y. Isoda, and S. Nakabayashi (2003), Control on dissolved iron concentrations in deep waters in the western North Pacific: Iron(III) hydroxide solubility, *J. Geophys. Res.*, *108*(C9), 3289, doi:10.1029/2002JC001481.
Laes, A., S. Blain, P. Laan, E. Achterberg, G. Sarthou, and H. deBaar (2003), Deep dissolved iron profiles in the eastern North Atlantic in relation to water masses, *Geophys. Res. Lett.*, *30*(17), 1902, doi:10.1029/2003GL017902.
Landing, W., and K. Bruland (1987), The contrasting biogeochemistry of iron and manganese in the Pacific Ocean, *Geochim. Cosmochim. Acta*, *51*, 29–43.
Landing, W., C. Measures, C. Buck, and M. Brown (2004), A North Atlantic Ocean section for dissolved Fe and Al, paper presented at ASLO/TOS 2004 Ocean Research Conference, Am. Soc. of Limnol. and Oceanogr., Honolulu, Hawaii.
Lefèvre, N., and A. J. Watson (1999), Modeling the geochemical cycle of iron in the oceans and its impact on atmospheric CO_2 concentrations, *Global Biogeochem. Cycles*, *13*, 727–736.
Liu, X., and F. Millero (2002), The solubility of iron in seawater, *Mar. Chem.*, *77*, 43–54.
Loscher, B., H. de Baar, J. de Jong, C. Veth, and F. Dehairs (1997), The distribution of Fe in the Antarctic circumpolar current, *Deep Sea Res., Part II*, *44*, 143–187.
Luo, C., N. Mahowald, and J. del Corral (2003), Sensitivity study of meteorological parameters on mineral aerosol mobilization, transport and distribution, *J. Geophys. Res.*, *108*(D15), 4447, doi:10.1029/2003JD003483.
Mackey, D., J. O'Sullivan, and R. Watson (2002), Iron in the western Pacific: A riverine or hydrothermal source for iron in the Equatorial Undercurrent?, *Deep Sea Res., Part I*, *49*, 877–893.
Marshall, J., A. Adcroft, C. Holl, L. Perelman, and C. Heisey (1997a), A finite-volume, incompressible Navier Stokes model for studies of the ocean on parallel computers, *J. Geophys. Res.*, *102*, 5753–5766.
Marshall, J., C. Hill, L. Perelman, and A. Adcroft (1997b), Hydrostatic, quasi-hydrostatic, and nonhydrostatic ocean modeling, *J. Geophys. Res.*, *102*, 5733–5752.
Martin, J. (1990), Glacial-interglacial CO_2 change: The iron hypothesis, *Paleogeography*, *5*, 1–13.
Martin, J., and S. Fitzwater (1988), Iron deficiency limits phytoplankton growth in the north-east Pacific subarctic, *Nature*, *331*, 341–343.
Martin, J., and R. Gordon (1988), Northeast Pacific iron distributions in relation to phytoplankton productivity, *Deep Sea Res., Part I*, *35*, 177–196.
Martin, J., G. Knauer, D. Karl, and W. Broenkow (1987), VERTEX: Carbon cycling in the northeast Pacific, *Deep Sea Res.*, *34*, 267–285.
Martin, J., R. Gordon, S. Fitzwater, G. Knauer, and W. Broenkow (1989), VERTEX: Phytoplankton/iron studies in the Gulf of Alaska, *Deep Sea Res.*, *36*, 649–680.
Martin, J., R. Gordon, and S. Fitzwater (1990), Iron in Antarctic waters, *Nature*, *345*, 156–158.
Martin, J., S. Fitzwater, R. Gordon, C. Hunter, and S. Tanner (1993), Iron, primary production and carbon-nitrogen flux studies during the JGOFS North Atlantic Bloom Experiment, *Deep Sea Res., Part II*, *40*, 115–134.
Martin, J., et al. (1994), Testing the iron hypothesis in ecosystems of the equatorial Pacific Ocean, *Nature*, *371*, 123–129.
Matsumoto, K., et al. (2004), Evaluation of ocean carbon cycle models with data-based metrics, *Geophys. Res. Lett.*, *31*, L07303, doi:10.1029/2003GL018970.
McKinley, G., M. Follows, J. Marshall, and S.-M. Fan (2003), Interannual variability of air-sea O_2 fluxes and the determination of CO_2 sinks using atmospheric O_2/N_2, *Geophys. Res. Lett.*, *30*(3), 1101, doi:10.1029/2002GL016044.
McKinley, G., M. Follows, and J. Marshall (2004), Mechanisms of air-sea CO_2 flux variability in the Equatorial Pacific and the North Atlantic, *Global Biogeochem. Cycles*, *18*, GB2011, doi:10.1029/2003GB002179.
Measures, C., and S. Vink (1999), Seasonal variations in the distribution of Fe and Al in the surface waters of the Arabian Sea, *Deep Sea Res., Part II*, *46*, 11,597–11,622.
Measures, C., and S. Vink (2001), Dissolved Fe in the upper waters of the Pacific sector of the Southern Ocean, *Deep Sea Res., Part I*, *48*, 3913–3941.
Michaels, A., D. Olson, J. Sarmiento, J. Ammerman, K. Fanning, R. Jahnke, A. Knap, F. Lipschultz, and J. Prospero (1996), Inputs, losses and transformations of nitrogen and phosphorus in the pelagic North Atlantic Ocean, *Biogeochemistry*, *35*, 181–226.
Mills, M., C. Ridame, M. Davey, J. L. Roche, and R. Geider (2004), Iron and phosphorus co-limit nitrogen fixation in the eastern tropical North Atlantic, *Nature*, *429*, 292–294.
Moore, J., S. Doney, J. Kleypas, D. Glover, and I. Fung (2002), An intermediate complexity marine ecosystem model for the global domain, *Deep Sea Res., Part II*, *49*, 403–462.
Najjar, R., J. Sarmiento, and J. Toggweiler (1992), Downward transport and fate of organic matter in the ocean: Simulations with a general circulation model, *Global Biogeochem. Cycles*, *6*, 45–76.
Nakabayashi, S., M. Kusakabe, K. Kuma, and I. Kudo (2001), Vertical distributions of Iron(III) hydroxide solubility and dissolved iron in the northwest North Pacific Ocean, *Geophys. Res. Lett.*, *28*, 4611–4614.
Nakabayashi, S., K. Kuma, K. Sasaoka, S. Saitoh, M. Mochizuki, N. Shiga, and M. Kusakube (2002), Variation in iron(III) solubility and iron concentration in the northwestern North Pacific Ocean, *Limnol. Oceanogr.*, *46*, 885–892.
Nishioka, J., S. Takeda, C. Wong, and W. Johnson (2001), Size-fractionated iron concentrations in the northeast Pacific Ocean: Distribution of soluble and small colloidal iron, *Mar. Chem.*, *74*, 157–179.
Nishioka, J., S. Takeda, I. Kudo, D. Tsumune, T. Yoshimura, K. Kuma, and A. Tsuda (2003), Size-fractionated iron distributions and iron-limitation processes in the subarctic NW Pacific, *Geophys. Res. Lett.*, *30*(14), 1730, doi:10.1029/2002GL016853.
Nolting, R., L. Gerringa, M. Swagerman, K. Timmermans, and H. de Baar (1998), Fe(III) speciation in the high nutrient, low chlorophyll Pacific region of the Southern Ocean, *Mar. Chem.*, *62*, 335–352.
Paltridge, G., and C. Platt (1976), *Radiative Processes in Meteorology and Climatology*, Elsevier, New York.
Parekh, P., M. Follows, and E. Boyle (2004), Modeling the global ocean iron cycle, *Global Biogeochem. Cycles*, *18*, GB1002, doi:10.1029/2003GB002061.
Petit, J., et al. (1999), Climate and atmospheric history of the past 420,000 years from the Vostok ice core, Antarctica, *Nature*, *399*, 429–436.
Powell, R., and J. Donat (2001), Organic complexation and speciation of iron in the south and equatorial Atlantic, *Deep Sea Res., Part II*, *48*, 2877–2893.
Price, N., L. Anderson, and F. Morel (1994), The equatorial Pacific Ocean: Grazer-controlled phytoplankton populations in an iron-limited ecosystem, *Limnol. Oceanogr.*, *39*, 520–534.
Roe, P. (1985), Some contributions to the modeling of discontinuous flows, in *Large-Scale Computations in Fluid Mechanics*, edited by B. Engquist, S. Osher, and R. Somerville, pp. 163–193, Am. Math. Soc., Providence, R. I.
Rue, E., and K. Bruland (1995), Complexation of iron(III) by natural organic ligands in the central North Pacific as determined by a new

competitive ligand equilibration/adsorptive cathodic stripping voltammetric method, *Mar. Chem.*, *50*, 117–138.
Rue, E., and K. Bruland (1997), The role of organic complexation on ambient iron chemistry in the equatorial Pacific Ocean and the response of a mesoscale iron addition experiment, *Limnol. Oceanogr.*, *42*, 901–910.
Sarthou, G., et al. (2003), Atmospheric iron deposition and sea-surface dissolved iron concentrations in the eastern Atlantic Ocean, *Deep Sea Res., Part I*, *50*, 1339–1352.
Sedwick, P., and G. DiTullio (1997), Regulation of algal blooms in Antarctic shelf waters by the release of iron from melting sea ice, *Geophys. Res. Lett.*, *24*, 2515–2518.
Sedwick, P., P. Edwards, D. Mackey, F. Griffiths, and J. Parslow (1997), Iron and manganese in surface waters of the Australian subantarctic region, *Deep Sea Res., Part I*, *44*, 1239–1253.
Sedwick, P., G. DiTullio, D. Hutchins, P. Boyd, F. Griffiths, A. Crossley, T. Trull, and B. Queguiner (1999), Limitation of algal growth by iron deficiency in the Australian subantarctic region, *Geophys. Res. Lett.*, *26*, 2865–2868.
Sedwick, P., G. DiTullio, and D. Mackey (2000), Iron and manganese in the Ross Sea, Antarctica: Seasonal iron limitation in Antarctic shelf waters, *J. Geophys. Res.*, *105*, 11,321–11,336.
Sohrin, Y., S. Iwamoto, M. Matsui, H. Obata, E. Nakayama, K. Suzuki, N. Handa, and M. Ishii (2000), The distribution of Fe in the Australian sector of the Southern Ocean, *Deep Sea Res., Part I*, *47*, 55–84.
Sunda, W., and S. Huntsman (1995), Iron uptake and growth limitation in oceanic and coastal phytoplankton, *Mar. Chem.*, *50*, 189–206.
Takata, H., et al. (2004), Spatial variability of iron in the surface water of the northwestern North Pacific Ocean, *Mar. Chem.*, *86*, 139–157.
Takeda, S., and H. Obata (1995), Response of equatorial Pacific phytoplankton to subnanomolar Fe enrichment, *Mar. Chem.*, *50*, 219–227.
Takeda, S., A. Kamatani, and K. Kawanobe (1995), Effects of nitrogen and iron enrichments on phytoplankton communities in the northwestern Indian Ocean, *Mar. Chem.*, *50*, 229–241.
Timmermans, K., L. Gerringa, H. de Baar, B. van der Wagt, M. Veldhuis, J. de Jong, and P. Croot (2001), Growth rates of large and small Southern Ocean diatoms in relation to availability of iron in natural seawater, *Limnol. Oceanogr.*, *46*, 260–266.
Trenberth, K., J. Olson, and W. Large (1989), A global ocean wind stress climatology based on ECMWF analyses, *Tech. Rep. NCAR/TN-338+STR*, Natl. Cent. for Atmos. Res., Boulder, Colo.
Tsuda, A., et al. (2003), A mesoscale iron enrichment in the western subarctic Pacific induces a large centric diatom bloom, *Science*, *300*, 958–961.
van den Berg, C. (1995), Evidence for organic complexation of iron in seawater, *Mar. Chem.*, *50*, 139–157.
Vink, S., and C. Measures (2001), The role of dust deposition in determining surface water distributions of Al and Fe in the south west Atlantic, *Deep Sea Res., Part II*, *48*, 2787–2809.
Watson, A., and J. Orr (2003), Carbon dioxide fluxes in the global ocean, in *Ocean Biogeochemistry: The Role of the Ocean Carbon Cycle in Global Change (a JGOFS Synthesis)*, edited by M. Fasham, pp. 123–141, Springer, New York.
Weeks, D., and K. Bruland (2002), An improved flow injection analysis method for the determination of iron in seawater, *Anal. Chim. Acta*, *453*, 21–32.
Wells, M., N. Price, and K. Bruland (1995), Iron chemistry in seawater and its relationship to phytoplankton: A workshop report, *Mar. Chem.*, *48*, 157–182.
Witter, A., and G. Luther (1998), Variation in Fe(III)-organic complexation with depth in the northwestern Atlantic Ocean as determined using a kinetic approach, *Mar. Chem.*, *62*, 241–248.
Witter, A., B. Lewis, and G. Luther (2000a), Iron speciation in the Arabian Sea, *Deep Sea Res., Part II*, *47*, 1517–1539.
Witter, A., D. Hitchins, A. Butler, and G. Luther (2000b), Determination of conditional stability constants and kinetic constants for strong model Fe-binding ligands in seawater, *Mar. Chem.*, *69*, 1–17.
Wu, J., and E. Boyle (1998), Determination of trace levels of iron in seawater by isotope dilution high resolution ICPMS, *Anal. Chim. Acta*, *267*, 183–191.
Wu, J., and E. Boyle (2002), Iron in the Sargasso Sea: Implications for the processes controlling dissolved Fe distribution in the ocean, *Global Biogeochem. Cycles*, *16*(4), 1086, doi:10.1029/2001GB001453.
Wu, J., and G. Luther (1994), Size-fractionated iron concentrations in the water column of the western North Atlantic Ocean, *Limnol. Oceanogr.*, *39*, 1119–1129.
Wu, J., and G. Luther (1995), Complexation of Fe(III) by natural organic ligands in the northwest Atlantic Ocean by a competitive ligand equilibration method and kinetic approach, *Mar. Chem.*, *50*, 159–177.
Wu, J., and G. Luther (1996), Spatial and temporal distribution of iron in the surface water of the northwestern Atlantic Ocean, *Geochim. Cosmochim. Acta*, *60*, 2729–2741.
Wu, J., E. Boyle, W. Sunda, and L. Wen (2001), Soluble and colloidal iron in the oligotrophic North Atlantic and North Pacific, *Science*, *293*, 847–849.
Yamanaka, Y., and E. Tajika (1997), Role of dissolved organic matter in the marine biogeochemical cycles: Studies using an ocean biogeochemical general circulation model, *Global Biogeochem. Cycles*, *11*, 599–612.

E. A. Boyle, M. J. Follows, and P. Parekh, Department of Earth, Atmospheric and Planetary Sciences, Massachusetts Institute of Technology, 54-1511, 77 Massachusetts Avenue, Cambridge, MA 02139, USA. (parekh@ocean.mit.edu)

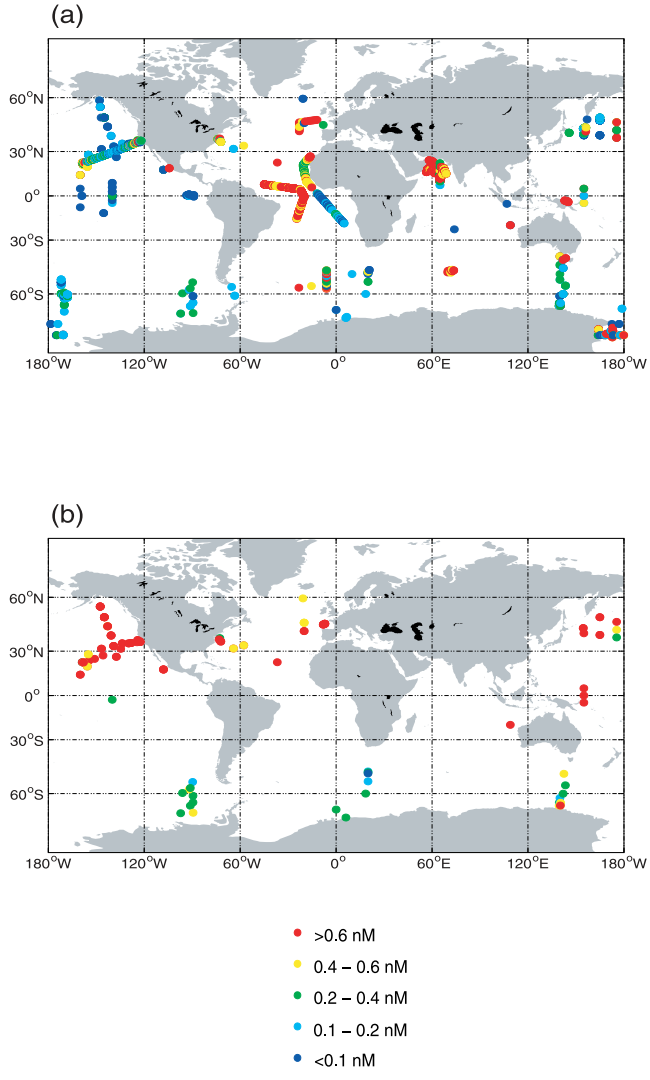

Figure 1. (a) Observed dissolved [*Fe*] (<0.4 μm) in surface waters (0 to 50 m) and (b) intermediate waters (800–1100 m). We have expanded the *Gregg et al.* [2003], *de Baar and de Jong* [2001], and *Johnson et al.* [1997] databases. References are found in Appendix A. The annotated and fully referenced data set is available for downloading at ocean.mit.edu/∼mick/Downloads.html.

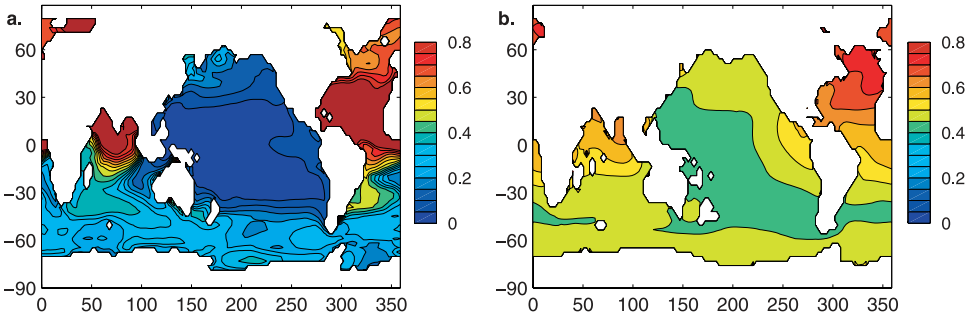

Figure 5. Annually averaged modeled [Fe_T] (nM) at (a) surface and (b) 935 m.

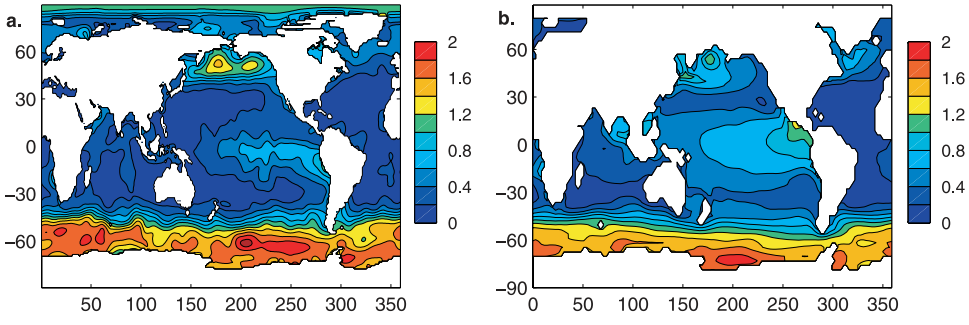

Figure 7. Annually averaged surface PO_4 (μM): (a) Climatology [*Conkright et al.*, 2002] and (b) model results.